Investigation on growth, structural, dielectric, optical and third-order optical nonlinear properties of 8-hydroxyquinolinium 4-chloro-3-nitrobenzoate 4-chloro-3-nitrobenzoic acid crystal

To cite this article before publication: G Ahila *et al* 2020 *Mater. Res. Express* in press https://doi.org/10.1088/2053-1591/ab676b

Investigation on growth, structural, dielectric, optical and third-order optical nonlinear properties of 8-hydroxyquinolinium 4-chloro-3-nitrobenzoate 4-chloro-3-nitrobenzoic acid crystal

G. Ahila[1], M. Divya Bharathi[1], J. Mohana[1], G. Vinitha[2], G.Anbalagan[3,*]

[1]Department of Physics, Presidency College, Chennai 600005 India

[2]Department of Physics, VIT University, Chennai 600127, India

[3,*]Department of Nuclear Physics, University of Madras, Chennai 600025, India

Abstract

An organic 8-hydroxyquinolinium 4-chloro-3-nitrobenzoate 4-chloro-3-nitrobenzoic acid (8-HQCN) was synthesized and the crystals were grown by employing solution growth method. Single crystal XRD data revealed crystal system (monoclinic, space group $P2_1/n$), and cell dimensions (a = 6.9806(2) Å, b = 11.9919(4) Å, c = 26.8872(8) Å). The FT-IR, FT-Raman and NMR spectral analyses provide the molecular structure. UV-Visible spectrum provides a band gap (3.03 eV) and cut off wavelength (404 nm) of the crystal. The broad emission at 580 nm in PL spectrum reveals the suitability of the material yellow light emission. Vicker's microhardness study gives the mechanical stability of the grown crystal. The nonlinear optical susceptibility ($\chi^{(3)}$) of the molecule was calculated as 16.78 $\times 10^{-6}$ esu from Z- scan technique and from DFT theory it was calculated to be 5.632 $\times 10^{-6}$esu using cam-b3lyp/6-311G (d, p). Thermo-optic coefficient of 8-HQCN was predicted to be 3.805×10^{-6} K^{-1} by thermal conductivity studies. This thermally prompted defocusing character can be made useful in optical limiters. The thermal investigation exhibits the bearing proficiency of 8-HQCN to be 127ºC. The orbital energy, band gap and the second hyperpolarizability were also studied by varying the applied field. The dispersion of the dielectric constant illustrates the usual behavior and the enhanced quality of the material gives the low dielectric loss. Antibacterial studies were taken to check the resistance to harmful bacteria of the grown crystal.

Keywords: Crystal structure; Vibrational analysis; Optical materials; Z-scan, Third order susceptibility

Corresponding author: +019487140051

E-Mail: anbu24663@yahoo.co.in (G.Anbalagan)

1. Introduction

Nonlinear-optics is an enticing domain of research exploration due to their broad range utilization in photonic devices. The quick nonlinear response, less costs, easy way by which the structure is tuned to manipulate either physicochemical properties which in turn enhances the NLO effect make the organic compounds beneficial over the inorganic materials [1,2]. The presence π-electron delocalization makes importance of many of the organic materials in designing the nonlinear optical devices [3,4]. The planarity [4, 5], functionalization with proper groups (e.g., π-electron rich) [3] and the di-radical character (DC) may add to large third-order NLO properties. Organic chromophores having a wider band gap are applicable for NIR photodetectors and NLO materials [6, 8]. The 8-hydroxyquinoline (8-HQ) contains a ring of phenol connected with a pyridine. The optical nonlinearity of 8-HQ can be notably refined on raising the accepting tendency of the pyridine and/or raising the donating tendency of the benzene ring. 8-hydroxyquinoline accept proton when reacts with acids and forms charge transfer compounds. In experimental and analytical point of view, the electroluminescent materials are established with 8-hydroxyquinoline. Hence, many researchers concentrate on studying 8-HQ related complex compounds [10-13]. Zidan et.al [14] reported the optical nonlinearity of 8-HQ with 2-chloroacetate and (2)-3-carboxyacryalate salts by Z-scan technique but their nonlinear optical susceptibility values are lower compared to the present work. Thirumurugan et.al [15] discussed the SHG property of 8-HQ with succinic acid. Similarly, on keeping 8-hydroxyquinoline as a base dibenzoyl (L)-tartaric acid [16], 3, 5-dinitrobenzoic acid [17] and picric acid [18], were reacted to form a pure crystal but its efficiency was discussed

only through linear optical absorption but not in its nonlinear optical property. Selvakumar et.al [19] has already reported the characterization of 8-hydroxyquinolinium 4-nitrobenzoate 4-nitrobenzoic acid crystal. Furthermore the optical third order nonlinearity has not been discussed. But the present work has more advantages over the others by exhibiting a higher value of third order nonlinear optical susceptibility and also it exhibits the optical limiting behavior. So far the reported papers mentioned have not reported about the optical limiting nature. In this context, the grown 8-HQCN crystal shines towards using it in applications over effect of lasers, the interaction between laser materials, in the outstanding field of information technology, which is inclusive of sensing, communicating, storing and processing of information. In this treatise, we communicate the structural analysis, optical, thermal and nonlinear activities of 8-hydroxyquinolinium 4-chloro-3-nitrobenzoate 4-chloro-3-nitrobenzoic acid (8-HQCN) single crystal. In addition, the theoretical study was also done to find out the orbital's energy, band gap and the second hyperpolarizability by varying the applied field and the nonlinear optical susceptibility was also found using DFT.

2. Materials and methods

2.1. Synthesis and crystal growth

The 8-hydroxyquinolinium 4-chloro-3-nitrobenzoate 4-chloro-3-nitrobenzoic acid (8-HQCN) was prepared from 8-hydroxyquinoline (Merck) and 4-chloro-3-nitrobenzoic acid (AR Grade, Sigma Aldrich) in the equimolar ratio. The 8-hydroxyquinoline gently added to the ethanol solution of 4-chloro-3-nitrobenzoic acid it with a continuous stirring. The small amount of double distilled water was poured to reduce the evaporation speed with the aim to yield good quality crystal. The 8-HQCN compound is feebly soluble in water, but highly in ethanol and methanol. However, good yield of crystals is being obtained using ethanol as a solvent. The solubility was tested from 30^{o}C. The equilibrium state of the solute for every 5^{o}C was found

using gravimetric analysis when the solution attains the saturation. The solubility curve attained for 8-HQCN is visualized in Fig.1 (a). The solubility curve shows the fitness of ethanol medium for the growth of 8-HQCN crystal from the slow evaporation method. The saturated solution was maintained at 35°C without disturbing. In a time of 30 days, a transparent crystal, with dimensions 8×4×1 mm^3 was collected from mother solution and shown in Fig.1 (b).

2.2. Experimental details

Bruker Kappa APEX II diffractometer with MoKα radiation of wavelength 0.71073Å was employed to study the crystal structure. The intensities of 4956 distinctive reflections were utilized out of the 18779 reflections in a limit of 1.52 to 27.16°. The structure was analyzed by direct method using SHELXL97 [20] to refine the structure with refinement value R= 0.0379 and $wR(F_2)$ = 0.0969 for the intensity $I>2\sigma(I)$. The FT-IR spectrum was obtained using PERKIN ELMER SPECTRUM one FT-IR spectrometer by employing KBr pellet technique. Mercury lamp was used as the source and the measurements were taken with a resolution of 1.0 $cm^{-1.}$ The spectrum was obtained in the wavelength range 4000-450 cm^{-1}. The BRUKER RFS 27: Stand alone FT-Raman Spectrometer equipped with Nd: YAG laser (wavelength 1064 nm) was employed to record the FT-Raman spectrum between 4000 and 50 cm^{-1} and the instrument has the resolution of 2.0 cm^{-1} .The NMR spectrum of 8-HQCN was obtained with BRUKER AMX 400 spectrometer using $CDCl_3$ as solvent and TMS as the internal standard. The transmittance spectrum in the range 190-900 nm was recorded using T+90 PG spectrophotometer instrument designed with deuterium and halogen source lamps. A well-polished crystal of thickness 1.2 mm was used for UV-Vis study. The photoluminescence (PL) spectrum was recorded with Perkin Elmer (LS-45) PL unit in the wavelength region 350 - 750 nm and the sample was excited at wavelength 430 nm. A well-polished, flat surface of 8-HQCN crystal was tested for hardness

properties using Vicker's indentation tester. The diagonal length of the impressions was noted for indentation loads 10, 25, 50 and 100 g at room temperature by keeping the indentation time as 10 s. The third-order nonlinear optical property was studied by Z- scan technique. Light from CW Nd: YAG Laser (532 nm) is directed upon the sample through a lens of focal length as 3.5 cm. The 8-HQCN crystal was retained in 1 mm width optical cell. The digital meter having a photo detector was utilized to record the transmittance from the beam from an aperture. The thermal conductivity of the powder 8- HQCN was measured using C-Therm TCi analyser. This acts on the theory of Modified Transient Plane Source Technique. The decomposition of the 8-HQCN molecule is monitored by heating the sample in NETZSCH STA 449 instrument. About 3.292 mg of the sample in an alumina crucible was heated at 20 K/min in nitrogen atmosphere. The dielectric measurements in the frequency region 50 Hz -5 MHz were done using an LCR meter at the temperatures 50°, 60°, 70° and 80°C. Silver paste was applied over the cut and polished 8-HQCN sample and placed in the cell which is connected with a thermocouple. The grown 8-HQCN compound was examined against *E. coli* NCIM 2931 and *S. Aureus bacteria* with implementing agar well diffusion technique. About 15-20mL of Nutrient agar was spilled on sterile disposable Petri dishes (90 mm) and was enabled to stiffen. 100µL of freshly cultured suspension of *E. coli* NCIM 2931 (middle of log phase) in nutrient broth was streaked over the external surface of the agar plate and spread uniformly using a sterilized glass rod (L-rod). Four sterile disks were smeared attentively on the exterior surface of the seeded agar plates with sterile forceps. Three blank disks were taken with 10 µL of sterile RO water and the trial sample with desperate concentrations (0.1, 0.5 and 1mM) was added to the different disks. The disks were allowed to incubate at 37°C for 24 hours and 48 hours. The diameter zones of

inhibition were measured and the analysis was executed in triplicate. Same test experiments were replicated with other bacterial species, *S. aureus.*

2.3. Computational details

The molecular geometry optimization, without symmetry restrictions, was performed using density functional theory (DFT) with the hybrid exchange correlation functional (CAM-B3LYP) and using the 6-311G (d, p) [21, 22] basis set. The Gaussian 09 package [23] was employed for the above calculation and molecule was visualized by Gauss View [24]. The TD-DFT) at B3LYP/6- 311++G (d, p) level of theory was employed to study the electronic absorption spectrum of the optimized molecule in gas and solvent (DMSO and chloroform) phases. The nature of the excited state, the oscillator strength (f_n), electronic excitation energies (E_{gn}) and the difference in dipole moment between ground and excited states ($\Delta\mu_{ng}$) were also obtained.

3. Results and Discussion

3.1. Crystal structure analysis

The crystal data of 8-HQCN crystal are represented in Table 1. From Table 1, one can infer that 8-HQCN belongs to the monoclinic system with space group $P2_1/n$ and the computed lattice constants are: a = 6.9806(2) Å, b = 11.9919(4) Å, c = 26.8872(8) Å and V= 2248.52(12) $Å^3$. The ORTEP and packing diagram are represented in Figs.2 and 3 while the Table 2 gives hydrogen bond geometry. In addition, the bond distances and bond angles are produced in Table S1 and the values about anisotropic parameters in Table S2 and the fractional atomic coordinates along with deracination parameters ($Å^2$) which are equally isotropic in Table S3. The 8-HQCN compound ($C_{23}H_{15}C_{l2}N_3O_9$), consist of a protonated 8-hydroxyquinolinium cation, 4-chloro-3-nitrobenzoate anion and a neutral 4-chloro-3-nitrobenzoic acid molecule being in the structural unsymmetrical unit. The unsymmetrical unit involves two aromatic loops of neutral 4-chloro-3-

nitrobenzoic acid molecule which is planar with 3.58(8)° dihedral angle. The networks of O—H···O, N—H···O and C—H···O hydrogen bonds stabilizes the 8-HQCN. The carboxylate (COO^-) oxygen atoms act like hydrogen bond acceptors, and 8-hydroxyquinolinium N atoms provide the most extensive part as donors in the network. Hydrogen bonding happens in every 8-hydroxyquinolinium hydrogen atoms as a donor. Furthermore, the carboxyl $O5^i$ atom involves one hydrogen bond as an acceptor with H1 atom from the 8-hydroxyquinolinium cation group. The nitro O7 atom of neutral 4-chloro-3-nitrobenzoic acid is connected to the H2 atom via C—H···O hydrogen bond (Table S1). The intermolecular C-H… O bonds connect the neighbouring cation and anion molecules into infinite one dimensional chains along a [1 0 0] axis. The chains connecting O-H… O and N-H… O form a three dimensional grid. Weak intermolecular π…π interactions exhibits in the structure. The C16-O3 (1.209(2) Å) and C16-O2H (1.316(2) Å) has typical bond lengths for C=O and C-OH respectively for COOH groups. The COOH group of 4-chloro-3-nitrobenzoic acid gets deprotonated, whereas the 8-hydroxyquinolinium group gets protonated at N2 position. The approximately equal bond lengths C23-O4 (1.239(2) Å) and C23-O5 (1.269(2) Å) are typical for the delocalized carboxylate COO^- groups. The data related to 8-HQCN have been submitted to the Cambridge Crystallographic Data Centre (**CCDC - 1405242**).

3.2. Functional group analysis

The information associated with the configuration of the molecule structure and nature of chemical bonds was identified by the modes of vibration. The recorded spectra are produced in Figs.4 and 5. The spot of the O-H bond relays upon the potency of hydrogen bonds abiding in the material. The broad O-H stretching normally expected between 2700 and 3540 cm^{-1}. The broad peak seen in FT-IR at 3433 cm^{-1} is accredited to O-H stretching of 8-hydroxyquinoline

[25]. The configuration of proton transfer is strongly evidenced by the N-H stretching vibration at 3091cm^{-1} in FT-IR and FT-Raman at 3078 cm^{-1} [13]. The 8-HQCN structure comprises of a COOH; COO^{-} of 4-chloro-3-nitrobenzoic acid where one is ionized and the other is neutral. The COOH stretching vibration of 4-chloro-3-nitrobenzoic acid moiety is observed around 1700 cm^{-1} in both the spectra. The peak occupying at 1595 cm^{-1} corresponds to asymmetric stretching while the one observed at 1400 cm^{-1} attributes the symmetric stretching of COO^{-} (Fig.4). These vibrations in FT-Raman spectrum were found at 1604 and 1432 cm^{-1} in FT-Raman spectrum [13]. The NO_2 asymmetric vibrations were present at 1533 cm^{-1} in FT-IR and at 1538 cm^{-1} present in FT-Raman and similarly corresponding symmetrical stretching in FT-IR occupied at 1350 cm^{-1} and in FT-Raman occupied at 1392 cm^{-1} [26]. The peaks detected at 2919 cm^{-1} and 2777 cm^{-1} in FT-IR and 2593 cm^{-1} in FT-Raman was attributed to C- H stretching vibrations. The C-H out of plane bending vibration was observed at 847 cm^{-1} [26]. The peak at 1523 cm^{-1} in FT-Raman is due to C=C bending vibration [27]. The phenolic C-O stretching creates a vibrational peak is recorded at 1267 cm^{-1} in FT-IR spectrum and 1272 cm^{-1} in FT-Raman [19]. The OH in plane distorting vibrations is accredited to the bands at 1306 cm^{-1} both the spectra of FT-IR and FT-Raman. The vibrational stretching is noticed at 1108 and 1041 cm^{-1} in the FT-IR and 1110, 1065 and 1045 cm^{-1} in FT-Raman corresponds to a C-Cl. The C-N deformation observed at 910 cm^{-1} and 912 cm^{-1} in FT-IR and FT-Raman spectrum respectively. The C-N stretching vibration is observed at 882 cm^{-1} in FT-IR and at 880 cm^{-1} in FT-Raman. There are out of plane bending vibrations found at 418 and 220 cm^{-1} in FT-Raman because of C-C-C, but these peaks are not seen in the IR spectra [13]. The vibrations noticed at 115 and 103 cm^{-1} are the lattice mode vibrations [28]. The vibrational assignments are compiled in Table 3.

3.3. NMR spectral analysis

The H^1NMR and C^{13} NMR spectrum are presented in Figs. 6 and 7 with the chemical diagram. A singlet (–CH) proton of 8-hydroxyquinoline appears at δ=9.828 ppm. The doublet observed at δ = 8.464 and 8.461ppm is due the aromatic protons. Similarly, the para position of 4-chloro 3-nitrobenzoic acid produces a singlet at δ = 8.830 ppm. The protons aromatic C-H of 8-HQ is noticed as singlet at δ = 7.07 ppm. The 4-chloro 3-nitrobenzoate acid ring produces a doublet at δ = 7.850 and 7.870 ppm The N^+H and OH of 8-hydroxyquinolinium moiety in the complex produces far down field shifted because of the nearby electron withdrawing group and therefore it does not exist in the spectrum [29]. The C=O bond of 8-hydroxyqunoline ring produces a signal at δ = 153.68 ppm. The C-C atoms linking two rings of 8-hydroxyquinoline (pyridinium and hydroxyl benzene rings) produces a chemical shift in δ = 129.24 ppm. The carbon atoms detected in the pyridinium ring in 8-hydroxyqunoline appears as individual peaks at δ = 122.27 and 131.67 ppm. The 8-hydroxyqunoline contains an OH group which produces a peak at δ = 118.16 ppm. The weak signal produced at δ =138.80 ppm is due to the aromatic C-H proton of 8-hydroxyqunoline. Similarly the intense peak produced at δ =132.71 ppm belongs to 4-chloro-3-nitrobenzoic acid ring. The -Cl bond and C-N bond of 4-chloro-3-nitrobenzoic acid were identified as shift near δ = 134.44 and δ = 148.52 ppm.

3.4. Optical studies

3.4.1. UV-visible absorbance spectral analysis

The absorption spectrum was taken between the region 250 - 450 nm for the donor, acceptor, and finally obtained charge transferred complex keeping ethanol as solvent which is provided in the Fig.8(a). A strong colour change is the evidence of charge transfer interactions between the solutions of donor and acceptor when they are mixed together. The spectra obtained

for charge transfer complex represent the absorption band at wavelength of 320 nm. This absorption is not due to the precursors and considered to be the results of charge transfer complex formation between the investigated 8-hydroxyquinoline and 4-chloro-3-nitrobenzoic acid [30]. The solvent contains low energy absorptions of donor and an acceptor which can be explained by charge transfer transitions which involves the excitation of an electron on the donor to an empty orbital on the acceptor [31].

3.4.2. UV-visible transmittance analysis

A material used for nonlinear devices needs lower cut off wavelength and large optical transmittance [32]. The crystal shows a cut-off wavelength of 404 nm [33]. The normalized transmittance spectrum is displayed in Fig. 8 (b). The transmission through the crystal occurs since the excitation of electrons when there light source is impended on the crystal. The excitation is observed from the non-bonding to anti bonding (n → π*). The linear absorption coefficient (α) can be expressed as,

$$\alpha = \frac{2.3026(1/T)}{t} \tag{1}$$

Tauc's plot [32] provides information about the optical energy band gap of the material which is given by the relation:

$$\alpha h\upsilon = A(h\upsilon - E_g)^m \tag{2}$$

where, h and υ represents their usual meanings while Eg represents the optical band gap respectively. Also, the index m characterizes the transmission types. In the present case, the transition is a direct allowed transition and hence m =1/2. The optical band gap was estimated by extrapolating linear part of the curve to x-axis $(\alpha h\upsilon)^2 = 0$ in Fig.8 (c) and the plot gives value as 3.03 eV. This wide band gap endows 8-HQCN suitable for optoelectronic

applications [34]. The refractive index is the ultimate property for an optical material. Reflectance (R) and refractive index (n_o) of the crystal in terms of α and transmittance are expressed as [35],

$$R = \frac{1 \pm \sqrt{1 - \exp(-\alpha t) + \exp(\alpha t)}}{1 - \exp(-\alpha t)} \quad (3)$$

and

$$n_o = \frac{-(R+1) \pm \sqrt{-3R^2 + 10R - 3}}{2(R-1)} \quad (4)$$

The refractive index (n_o=3.05) of 8-HQCN at 532 nm crystal suggests that the material will enhance the performance of optical and photovoltaic devices such as solar cells [36], Bragg gratings [37], photonic crystals [38] and waveguide-based optical circuits [39].

3.5 Photoluminescence spectral analysis

The photoluminescence excitation and emission spectrum was recorded in the range between 200 and 800 nm and it is shown in Fig. 9. Excitation and emission wavelength were obtained by varying the excitation wavelength under a fixed emission wavelength and vice versa. However the present spectrum (Fig.9) an intense broad emission band around 580 nm which arises due to π*–n transitions of the carbonyl group in 4-chloro-3-nitrobenzoic acid of the 8HQCN crystal. Further the broadening of the emission band is associated with the population of various vibrational levels of the excited states. These broad yellow emission bands suggest that the 8HQCN crystal can serve as a potential photoactive material for a new tunable laser system and also to fabricate yellow lasers [40].

3.6. Mechanical studies

The mechanical stability is more important as concerned with the applications such as for the fabrication of devices. The hardness number (Hv) of the crystal is expressed as:

$$\mathrm{Hv} = 1.8544 \frac{P}{d^2} (kg / mm^2) \quad (5)$$

In the above equation P represents the load and d represents the diagonal length in μm. From the Fig.10 (a) it is seen that hardness number (H_V) rises linearly with load (P) and this trend is called as RISE (reverse indentation size effect) [41]. Due to the internal stress there is a crack observed at a load of 100 g [42]. Meyer's law states that [43],

$$\log P = \log k + n \log d \quad (6)$$

where k is the material constant. The work hardening coefficient is the slope of the straight line of log d - log P plot (Fig. 10b) and it is n = 3.35. The value of 'n' is supposed to lie between 1 and 1.6 for hard materials and the values exceeding more than 1.6 are categorized to be soft materials [44]. The value of n (=3.35) for the as grown 8HQCN suggests that it is a softer material. The selection of a material for device fabrication depends on fracture toughness (Kc) where the load exceeds the limit or yield point. The Kc ($g/\mu m^{3/2}$) can be computed from the following relation:

$$\frac{P}{l^{3/2}} = \beta_o \, \mathrm{K}_c ; \, l \geq \frac{d}{2} \quad (7)$$

l is half the length of the diagonal indentation mark and βo=7 for diamond indenter. The variation of Kc value at each load is shown in Fig. 11(a). It gives the knowledge of the depth of penetration of the indenter into the material's surface [45]. Brittleness is a measure of fracture induced in a material without appreciable deformation. Brittleness index Bi ($1/\mu m^{1/2}$) is given by the relation:

$$B_i = \frac{H_V}{K_c} \tag{8}$$

The variation of brittleness index with load for crystals is shown in Fig. 11 (b). The packing density of bonding between the neighboring atoms can be established by the elastic constant C_{11} was also calculated using Wooster's empirical formula:

$$C_{11} = \left(H_V\right)^{7/4} \tag{9}$$

The yield strength σ_v is given by the relation [46].

$$\sigma_y = \frac{H_V}{3}(n \geq 2) \tag{10}$$

Table 4 provides various mechanical parameters of 8HQCN and the high value of hardness number shows that the material can withstand while polishing for laser experiments.

3.7. Nonlinear optical study

3.7.1. Z-scan analysis

The Z-scan study [47] proves to be one of the best approaches to gain knowledge of the nonlinear index of refraction (n_2) and nonlinear absorption (β). The Z-scan analysis optimization parameters are given in the Table 5. The theoretical and experimental curve for closed aperture, open aperture and the proportion between closed and open aperture are shown in Figs.12-14. In the closed aperture figure, it is noticed that the peak pursued by a valley normalized transmittance interpreting the negative sign for nonlinearity refraction which is mentioned to be as self- defocusing effect. $\Delta T_{\text{p-v.}}$, the separation of normalized peak and valley transmittance is given by:

$$\Delta T_{p-v} = 0.406\left((1-S)^{0.25}\right)|\Delta\phi_0| \tag{11}$$

The linear aperture transmittance,

$$S = 1 - \exp\left(\frac{-2r_a^2}{\omega_a^2}\right) \tag{12}$$

where r_a denotes the aperture radius while ω_a radius of laser spot back the aperture. The nonlinear refractive index (n_2) [48] is given by:

$$n_2 = \frac{|\Delta\phi_0|}{kL_{eff}I_0} \tag{13}$$

L_{eff} is given as $L_{eff} = \left(\frac{1-e^{-\alpha L}}{\alpha}\right)$ with L denoting the length of the sample, α as the linear absorption coefficient, at the axis of focal point z = 0, and the wave vector $k = \frac{2\pi}{\lambda}$.

Theoretically the normalized transmittance can also be obtained for open and closed curvature with the help of following two equations:

$$T_{OA}(Z, S=1) = \sum_{m=0}^{\infty}\left(\frac{[q_0(Z,0)]^m}{(m+1)^{3/2}}\right) \quad \text{, where } q_0 = \frac{\beta I_0 L_{eff}}{1 + Z^2/Z_0^2} \tag{14}$$

$$T_{CA}(Z, \Delta\Phi_0) = 1 - \frac{4x\Delta\Phi_0}{(x^2+1)(x^2+9)} \tag{15}$$

Where Z places the sample position and Z_0^2 is the Rayleigh range of the beam and is given by

$$Z_0^2 = \frac{2\pi\omega_0^2}{\lambda} \tag{16}$$

The nonlinear absorption coefficient β is calculated from the following equation:

$$\beta = \frac{2\sqrt{2}\Delta T}{I_0 L_{eff}} \tag{17}$$

The Rayleigh length, $Z_R = \frac{k\omega_o^2}{2}$, where ω_o is the beam waist at focal spot. The real part (Re $\chi^{(3)}$) and the imaginary part (Im $\chi^{(3)}$) [49] bestowing to the subsequent relation:

$$\mathrm{Re}\,\chi^{(3)}(esu) = \frac{10^{-4}\left(\varepsilon_0 C^2 n_0^{\,2} n_2\right)}{\pi}\left(cm^2/W\right) \tag{18}$$

$$\mathrm{Im}\,\chi^{(3)}(esu) = \frac{10^{-2}\left(\varepsilon_0 C^2 n_0^{\,2} \lambda\beta\right)}{4\pi^2}\left(cm/W\right) \tag{19}$$

where ε_o, c are the universal constants, n_o is the linear index of refraction of the sample and λ is the wavelength of the laser beam.

From equations (18) and (19), third order nonlinear susceptibility is given by:

$$\left|\chi^3\right| = \left[\left(\mathrm{Re}\left(\chi^3\right)\right)^2 + \left(\mathrm{Im}\left(\chi^3\right)\right)^2\right]^{1/2} \tag{20}$$

The calculated the values of n_2,β, Re $\chi^{(3)}$ and Im $\chi^{(3)}$ are compared with the literature values which are specified in Table 6 [50-52]. Finally the effective nonlinear optical susceptibility calculated as 16.78×10^{-6} esu. One can understand from the Table 6 that the effective values of ($\chi^{(3)}$) and (γ) can be attributed to the delocalized π-electron configurations, and also the effective protonation process occurred in the crystal structure would enhance the third - order optical nonlinearities. The saturation absorption leads to nonlinear absorption and refraction attributing to the self defocusing in 8-HQCN crystal. The optical limiting curve for 8-HQCN crystal is represented in Fig.15. When input intensity increases the output intensity also rises linearly up to 27.4 mW and saturation is reached to a certain value. These outcomes are possibly used in nonlinear optical devices equally preventive in optical damage to the sensitive sensors [53].

The n_2 value acquired has its benefaction of noticeable origins on thermal effects or electronic effect. It is well established that refractive depends on temperature which is origin for nonlinearity and hence thermal origin is taken. CW lasers were used as a source of excitation in the current situation, the source of nonlinearity was solely thermal, and the sample acted as a thermal lens [54]. The laser heating leads to the generation of acoustic wave that changes the medium density followed by a variation of refractive index [55, 56]. The expression connecting thermal nonlinearity and thermo optic coefficient is depicted as below:

$$\frac{dn}{dT} = \frac{4n_2 K}{\alpha_0 \omega_0^{\,2}} \tag{21}$$

where dn/dT is the thermo- optic coefficient which is the differential of temperature dependable refractive index, ω_o owes to the waist of laser beam, n_2 and K the thermal conductivity of 8-HQCN respectively. The thermal conductivity (κ) of 8-HQCN was predicted as 0.073 ± 0.0037 W $m^{-1}K^{-1}$ at 50°C. By making use of κ, the thermo-optic coefficient was calculated as 3.805×10^{-6} K^{-1}. The material's polarizability and thermal expansion will cause this result. The self-defocusing effect exhibits in 8-HQCN crystal is ascertained to the thermal effect of continuous wave Nd: YAG laser beam of wavelength 532 nm which makes a spatial distribution of temperature in the crystal. The temperature dependent refractive index will cause optical nonlinearity. The fundamental investigation of thermal-induced nonlinearity will be valuable in better understanding the physics inherent of the nonlinear optical properties of materials. Moreover, thermal lens effect has found valuable application in measurement of weak absorption [57]. It is known that the NLO response of 8-HQCN is initiated from a structure factor [58] and the enhanced optical nonlinearities due to their expanded π-electron system [59-61].

3.7.2. Theoretical analysis

DFT is an efficient tool for the prediction of the NLO properties of macroscopic systems at low computational cost with electron-correlation effects [62]. The finite-field (FF) approach employed in first-principle techniques are the effectively applied in the investigation of NLO response since it illustrates the various electronic-structure techniques to estimate the NLO coefficients [63]. The induced molecular polarization can be articulated by a power series:

$$P_i = \sum_i \alpha_{ij} E_j + \sum_{jk} \beta_{ijk} E_j E_k + \sum_{jkl} \gamma_{ijkl} E_j E_k E_l + \cdots\cdots \quad (22)$$

Where the polarization P_i induced along the i^{th} molecular axes due to the electric field, Ej in the j^{th} direction, and α, β, γ are the linear, first and second order polarizability tensors respectively. The average second order hyperpolarizability (γ) is given by the expression:

$$\gamma_{tot} = \frac{1}{5}\left[\gamma_{xxxx} + \gamma_{yyyy} + \gamma_{zzzz} + 2\left(\gamma_{xxyy} + \gamma_{xxzz} + \gamma_{yyzz}\right)\right] \quad (23)$$

The molecular geometry optimization is shown in Fig.16. The average static second order hyperpolarizabillity was estimated to be $\gamma_{tot}(0;0,0,0) = 43.542\times10^{-36}$ esu. The π-conjugation of organic molecules enacts a climactic lead for acquiring third order nonlinearities. The charge transfer is more stabilized on enhancing the γ values and raise γ values arises from the hydrogen bonds of 8-HQCN and hence gives the NLO property [64, 65]. Normally, the apparent static third order susceptibility $\chi^{(3)}$ can be specified by the ensuing expression, $\chi^{(3)} = M\left[\frac{(n_r+2)}{3}\right]^4 \langle\gamma\rangle$, where M is number density of atoms and n_r be the refractive index of the crystal. In the above relation, the local-field alterations in the Lorentz approximation are also taken into account [66] and the calculation gives $\chi^{(3)}$ as 0.5632×10^{-5}esu.

Fig.16 shows the dependence of second hyperpolarizability on frequency and is seen that the electro-optical Kerr effect ($\langle\gamma(-\omega;\omega,0,0)\rangle$) and the electric-field-induced second-harmonic

generation (<γ(− 2ω;ω,ω,0)>) increase to a different extent with frequency. The energy gap (E_{HL}) plays significant reflects role in enhancing the optical properties [67]. The Fig.17 clearly shows the influence of external electric field on the energy distribution around the HOMO and LUMO along different directions. The decrease of band gap with the increase of the frequency of the applied field leads to the increase of <γ>. The value of EHL and <γ> are found to be 3.557 eV and 43.542×10^{-36} esu, respectively. Moving from the field Fx =0 to Fx= 0.03 and 0.06 au, the E_{HL} value reduces by 1.027 and 0.899 eV whereas the <γ>value increases by 21.09×10^{-6} esu and 77.98×10^{-6} esu, respectively. When moving from the zero-field to Fy= 0.03 and 0.06 au, the E_{HL} value reduces to 2.687 and 1.475 eV whereas the <γ> value increases by 96.5 $\times10^{-6}$ esu and -67.74×10^{-2} esu, respectively. A similar effect was observed when moving from the zero-field to Fz= 0.03 and 0.06 au, the E_{HL} value reduces to 3.209 and 1.459 eV whereas the <γ> value increases by 9.16×10^{-6} esu and 59.86×10^{-6} esu, respectively (Table 7).

Bai et al [68] established that the external electric field induces the changes in electron-density distribution on the molecules which in turn increases <γ>. It is also seen from Fig.18, there is a reduction and enlargement of lobes in the positive and negative direction of the electric field respectively, in HOMO. However, when Fx= 0.06 au lobes of the LUMO are pushed strongly along the positive direction of the electric field. This charge transfer enhancement produces a highly polarized electron density distribution responsible for the higher NLO response [69] which proves that external electric field can also tune the NLO properties.

3.8. Electronic excitation

Fifty excited states were identified and some of the excited states with k values having significant contributions are listed in Table 8. From the table it is noticed that the state 1st, 13^{th}, 14^{th} and 19^{th} have larger k values making dominant contributions to β values. Major contribution

is from 13th state which emanate owing to the excitation of charges from HOMO - 6 to LUMO +1 which belongs to the transition occurring between the orbital composed of 4-chloro-3-nitrobenzoate group to that of NO_2 group. The next major contribution is found in 14th and 19th state where the charges excite from HUMO – 5 to LUMO + 4 owing to the charge transfer between the 4-chloro-3-nitrobenzoate to the carboxyl group. 1st state contributes to β values between HUMO – 6 to LUMO + 0 in reasons with the nitrobenzoic group present in the 8-HQCN compound. Moderate k values of 4th, 5th, 6th and 8th state are due to the transitions occurring in 8-hydroxyquinoline molecule.

3.9. Thermal analysis

The TG-DTA curve shown in Fig.19 indicates that the crystal is stable up to 120°C. A small inflection around 120°C in TGA matches with a DTA peak 127°C. TGA curve shows single stage decomposition between 198°C and 317°C and this corresponds to the liberation of major organic molecules of the 8-HQCN compound. Thus, 8-HQCN is stable up to 120°C and the crystal can be implemented for various solid state applications.

3.10. Dielectric studies

The dielectric analysis of a material is an essential characterization to avail the details of the electrical properties of the material. Dielectric constant can be related to dimensions (thickness & area of the sample) and capacitance of the sample (C):

$$\varepsilon' = \frac{Ct}{\varepsilon_0 A} \tag{24}$$

$$\frac{\varepsilon''}{\varepsilon'} = \tan\delta \tag{25}$$

where ε_o is the permittivity of free space. Fig. 20(a) shows the normal behavior of the dielectric dispersion and the dispersion was large at lower frequency while being constant at higher frequency. The dielectric permittivity will be originated from electronic, ionic, orientation and space polarization mechanisms within the material. The high ε' at low frequencies originate from the accumulation of charges and theses charges will follow the applied electric field while the lagging of dipoles with electrical field tends decrease ε' with frequency. Moreover, dielectric constant almost constant in the region 1 kHz to 2 MHz due to the disappearance of space charge polarization in this frequency region. The observed low value of dielectric constant establishes that the as-grown crystal has potential for microwave applications. Similarly, the dielectric loss (ε") is higher at low frequency (Fig.20 (b)) attributes the oscillation of dipoles. The low value of (ε") proves the quality of the crystal [70]. Thus the material satisfies one of basic needs of photonic, electro-optic and NLO devices [71].

3.11. Antibacterial activity

The 8-hydroxyquinoline complexes are well entrenched for its antibacterial activity. The 8-HQCN was proved to be antibacterial resistant on testing for the species *E. coli* NCIM 2931 and *S. Aureus.* This antibacterial resistant activity of 8-HQCN is depicted in Fig.21 and also noted that the measured diameter of the zone after inhibition endured to be same after 24 hours and 48 hours of incubation. The measurement table of diameter of zone of inhibition coursed 8-HQCN against bacteria is given in Table 9. The higher concentration has a larger diameter of zone of inhibition than the lower concentration. Therefore, antibacterial analysis proves that 8-HQCN exhibits good resistance towards the harmful bacteria and hence applicable for medical and bio-medical applications.

4. Conclusion

The structure, lattice constants and the crystal system were obtained from the single crystal XRD analysis. The cut-off wavelength and band gap of the crystal was found by using transmittance spectrum and the absorption spectrum shows the charge transfer of 8HQCN. The molecular structure was well established by the spectral analyses. The photoluminescence of the crystal revealed yellow emission. Mechanical strength of the crystal is revealed from mechanical studies. Z-scan technique was exploited to study nonlinear parameters of the crystal. The thermo-optic effect causes the nonlinearity which helps to implement it to the optical application oriented devices. It is to be noted that reverse saturable absorption establishes the optical limiting effect and hence this material is useful for optical limiting applications. DFT was applied to estimate the theoretical third order nonlinear optical parameters. Also, the theoretical powers and experimental powers of $\chi^{(3)}$ were compared and were affirmed to be in good agreement. The 8-HQCN exhibits high withstanding thermal capacity up to 127°C. The charge relegation inside the molecule is shown on lowering HOMO-LUMO gap. The applied electric field strongly affects the band gap and hence second order hyperpolarizability. The low dielectric permittivity and the low dielectric loss enhance the optical quality of the material with lesser imperfections. Antibacterial study for the powdered sample was executed and was found that 8-HQCN exhibit good resistance towards the harmful bacteria.

References

[1] S.A. Sarkar, J.J. Pak, G.W. Rayfield, M.M. Haley, "Nonlinear Optical Properties of Dehydrobenzo 18 Annulenes: Expanded Two-Dimensional Dipolar and Octupolar NLO Chromophores," *J. Mater. Chem.* 11 (2001) 2943−2945.

[2] E. Benassi, F. Egidi, V. Barone, "General Strategy for Computing Nonlinear Optical Properties of Large Neutral and Cationic Organic Chromophores in Solution," *J. Phys. Chem. B* 119 (2015) 3155−3173.

[3] W.J. Nie, "Optical Nonlinearity - Phenomena, Applications, and Materials," *Adv. Mater.* 5 (1993) 520−545.

[4] M. Lanata, C. Bertarelli, M.C. Gallazzi, A. Bianco, M. DelZoppo, G. Zerbi, "Molecules with Quinoid Ground State: A New Class of Large Molecular Optical Nonlinearities," *Synth. Met.* 138 (2003) 357−362.

[5] S.Di Bella, "Second-Order Nonlinear Optical Properties of Transition Metal Complexes," *Chem. Soc. Rev.* 30 (2001) 355−366.

[6] Shijun Zheng , Amalia Leclercq , Jie Fu , Luca Beverina , Lazaro A. Padilha , Egbert Zojer , Karin Schmidt, Stephen Barlow, Jingdong Luo, Sei-Hum Jiang, Alex K.-Y. Jen , Yuanping Yi , Zhigang Shuai , Eric W. Van Stryland , David J. Hagan , Jean-Luc Brédas, Seth R. Marder, "Two-Photon Absorption in Quadrupolar Bis(Acceptor)-Terminated Chromophoreswith Electron-Rich Bis(Heterocycle)Vinylene Bridges," *Chem. Mater.* 19 (2007) 432 − 442.

[7] Aggelos Avramopoulos, Heribert Reis, Nicolás Otero, Panaghiotis Karamanis, Claude Pouchan, and Manthos G. Papadopoulos, "A Series of Novel Derivatives with Giant Second Hyperpolarizabilities, Based on Radiaannulenes, Tetrathiafulvalene, Nickel Dithiolene, and Their Lithiated Analogues," *J. Phys. Chem. C* 120 (2016) 9419 − 9435.

[8] Y.Yao, Y.Y. Liang, V. Shrotriya, S.Q. Xiao, L.P. Yu, Y. Yang, "Plastic near-Infrared Photodetectors Utilizing Low Band Gap Polymer," *Adv. Mater.* 19 (2007) 3979 − 3983.

[9] Mathias M. Schulze, Uwe Bohme, Anke Schwarzer, Edwin Weber, "Intermolecular interactions in the solid state structures of neutral and N-protonated 5-alkoxymethyl-8-hydroxyquinolines," *J. Mol. Struct.* 1133 (2017) 307 - 319.

[10] S. Franklin, T. Balasubramanian, "Salts of maleic and fumaric acids with oxine: the role of isomeric acids in hydrogen-bonding patterns," *Acta Cryst. C* 65 (2009) o58 – o61.

[11] G. Peramaiyan , P.Pandi, N.Vijayan, G. Bhagavannarayana , R. Mohan Kumar, "Crystal growth, structural, thermal, optical and laser damage threshold studies of 8-hydroxyquinolinium hydrogen maleate single crystals," *J. Cryst. Growth* 375 (2013) 6 – 9.

[12] M. Rajasekaran, P. Anbusrinivasan, S.C. Mojumdar, "Growth, spectral and thermal characterization of 8-hydroxyquinoline," *J. Therm. Analysis and Calorimetry* 100 (2010) 827–830.

[13] N. Sudharsana, V. Krishnakumar, R. Nagalakshmi, "Synthesis, experimental and theoretical Studies of 8-hydroxyquinolinium 3, 5-dinitrobenzoate single crystal," *J. Cryst. Growth* 398 (2014) 45-57.

[14] M.D. Zidan, A.Arfan, A.Allahham, D.Naima, "Investigation of optical nonlinearity of 8-hydroxyquinolinium 2-chloroacetate and 8-hydroxyquinolinium (Z)-3-carboxyacrylate salts by Z-scan technique," *Opt. Laser Technol.* 76 (2016) 85–90.

[15] R. Thirumurugan, B. Babu, K. Anitha, J. Chandrasekaran, "Investigation on growth, structure and characterization of succinate salt of 8-hydroxyquinoline: An organic NLO crystal," *Spectrochim. Acta A* 140 (2015) 44–53.

[16] N. Sudharsana V. Krishnakumar R. Nagalakshmi, "Experimental and theoretical investigations of non-centrosymmetric 8-hydroxyquinolinium dibenzoyl-(L)-tartrate methanol monohydrate single crystal," *J. Mater. Res. Bull.* 61 (2015) 136-145.

[17] N. Sudharsana, V. Krishnakumar, R. Nagalakshmi, "Synthesis, Experimental and Theoretical Stu- dies of 8-hydroxyquinolinium 3, 5- dinitrobenzoate single crystal," *J. Cryst. Growth* 398 (2014) 45-57.

[18] V. Krishna Kumar, R. Nagalakshmi, "Vibrational spectroscopic studies of an organic non-linear optical crystal 8-hydroxyquinolinium picrate," Spectrochim. *Acta Part A: Mol. Biomol. Spectrosc.* 66.4 (2007) 924-934.

[19] E. Selvakumar, G. Anandhababu P.Ramasamy, Rajnikant, V. Murugesan, A. Chandramohan, "Synthesis, growth and spectroscopic investigation of an organic molecular charge transfer crystal: 8-Hydroxyquinolinium 4-nitrobenzoate 4-nitrobenzoic acid," *Spectrochim. Acta A* 117 (2014) 259-263.

[20] G.M. Sheldrick, "A short history of SHELX," *Acta Cryst. A* 64 (2008) 112‑122.

[21] C. Lee, W. Yang, R.G. Parr, "Development of the Colle-Salvetti correlation-energy formula into a functional of the electron density," *Phys. Rev. B* 37 (1988)785-789.

[22] T. Yanai, D.P. Tew, N.C. Handy, "A new hybrid exchange–correlation functional using the Coulomb-attenuating method (CAM-B3LYP)," *Chem. Phys. Lett.* 393 (2004)51–57.

[23] M. J. Frisch, G. W. Trucks, H. B. Schlegel, G. E. Scuseria, M. A. Robb, J. R. Cheeseman, G. Scalmani, V. Barone, B. Mennucci, G. A. Petersson, H. Nakatsuji, M. Caricato, X. Li, H. P. Hratchian, A. F. Izmaylov, J. Bloino, G. Zheng, J. L. Sonnenberg, M. Hada, M. Ehara, K. Toyota, R. Fukuda, J. Hasegawa, M. Ishida, T. Nakajima, Y. Honda, O. Kitao, H. Nakai, T. Vreven, J. A. Montgomery, Jr., J. E. Peralta, F. Ogliaro, M. Bearpark, J. J. Heyd, E. Brothers, K. N. Kudin, V. N. Staroverov, T. Keith, R. Kobayashi, J. Normand, K. Raghavachari, A. Rendell, J. C. Burant, S. S. Iyengar, J. Tomasi, M. Cossi, N. Rega, J. M. Millam, M. Klene, J. E. Knox, J. B. Cross, V. Bakken, C. Adamo, J. Jaramillo, R. Gomperts, R. E. Stratmann, O. Yazyev, A. J. Austin, R. Cammi, C. Pomelli, J. W. Ochterski, R. L. Martin, K. Morokuma, V.

G. Zakrzewski, G. A. Voth, P. Salvador, J. J. Dannenberg, S. Dapprich, A. D. Daniels, O. Farkas, J. B. Foresman, J. V. Ortiz, J. Cioslowski, and D. J. Fox, Gaussian, Inc., Wallingford CT, 2013.

[24] Roy D. Dennington II,Todd A. Keith, John M. Millam, Gauss View 5.0, Gaussian, Inc., Wallingford CT, 2013.

[25] V. Krishnakumar, R. Nagalakshmi, P. Janaki, "Growth and spectroscopic characterization of a new organic nonlinear optical crystal - 8-hydroxyquinoline," *Spectrochim. Acta A* 61 (2005) 1097–1103.

[26] S. Sudhakar, M. Krishna Kumar, B.M.Sornamurthy, R.Mohan Kumar, "Synthesis, crystal growth, structural, thermal, optical and mechanical properties of solution grown 4-methylpyridinium 4-hydroxybenzoate single crystal," *Spectrochim. Acta A* 118 (2014) 929-937.

[27] L. Mariappan, A. Kandasamy, M.Rathnakumari, P.Suresh Kumar, "Synthesis, growth and properties of a novel organic nonlinear optical material: Benzimidazolium perchlorate," *Optik* 124 (2013) 5707-5710.

[28] T. Dhanabal, G. Amirthaganesan, M. Dhandapani, Samar K. Das, "Spectral, crystal structure, thermal and antimicrobial characterization of an organic charge transfer complex-3,5-dimethylpyrrazolinium picrate," *J. Mol. Struct.*1035 (2013) 483-492.

[29] Yusuf Atalay, Davut Avc, Adli Basoglu, "Molecular structure, vibrational and chemical shift assignments of 8-hydroxy-1-methylquinolinium iodide hydrate by density functional theory (DFT) and ab initio Hartree - Fock (HF) calculations," *Spectrochim. Acta A* 71 (2008) 760-765.

[31] R. S. Mulliken, "Structures of complexes formed by halogen molecules with aromatic and with oxygenated solvents," *J. Am. Chem. Soc.* 72 (1950) 600 – 608.

[30] A. A. Ibrahim, "Spectrophotometric studies of charge transfer complex of 8-hydroxyquinoline with 1, 4-benzoquinone," *Afr. J. Pure Appl. Chem.*5 (2011) 507–514.

[32] T. Balakrishnan, K. Ramamurthy, "Crystal growth, structural, optical, mechanical and thermal properties of a new nonlinear optical single crystal: L-Ornithine monohydrochloride," *Spectrochim. Acta A* 72 (2009) 269-273.

[33] V.G. Dmitriev, G.G. Gurzadyan, D.N. Nikoyosyan, "Hand Book of Nonlinear Optical Crystals", *Springer*, Berlin, 1999.

[34] Mohd. Shkir B. Riscob, Mohd. Hasmuddin, Preeti Singh, V. Ganesh, M.A. Wahab, Ernesto Dieguez, G. Bhagavannarayana, "Optical spectroscopy, crystalline perfection, etching and mechanical studies on p-nitroaniline (PNA) single crystals," *Opt. Mater.* 36 (2014) 675–681.

[35] G.Ahila, M. Divya Bharathi, J. Mohana, G. Vinitha, G. Anbalagan, "Growth, optical, mechanical and nonlinear optical properties of Furfurylaminium 2-chloro-5-nitrobenzoate single crystal," *Mater. Res. Express* 6 (2019) 045102.

[36] Bayram Gunduz, "Optical properties of poly [2-methoxy-5-(3′,7′-dimethyloctyloxy)-1,4-phenylenevinylene] light-emitting polymer solutions: effects of molarities and solvents," *Polym.Bull.*72 (2015) 3241-3267.

[37] A. Cusano, A. Iadicicco, D. Paladino, S. Campopiano, A. Cutolo, M. Giordano, "Micro-structured fiber Bragg gratings. Part II: Towards advanced photonic devices," *Opt. Fiber Technol*. 13 (2007) 291–301.

[38] T. Kohoutek, J. Orava, T. Sawada, H. Fudouzi, "Inverse opal photonic crystal of chalcogenide glass by solution processing," *J. Colloid. Interface Sci.* 353 (2011) 454-458.

[39] .F.Ho, M.A.Uddin, H.P.Chan, "The stability of high refractive index polymer materials for high-density planar optical circuits," *Polym. Degrad. Stab.* 94 (2009)158–161.

[40] M. A. F. M. da Silva, I.C.S. Carvalho, N. Cella, H.N. Bordallo, L.P. Sosman, "Evidence of broad emission band in the system $MgGa_2O_4$–Ga_2O_3 doped with Cr^{3+} ions," *Opt. Mater.* 35 (2013) 543–546.

[41] A. Philominal, S. Dhanuskodi, J. Philip, "Optical, thermal and microhardness studies on dichloridobis (1-ethyl-2, 6-dimethylpyridinium-4-olate-kO) zinc (II)," *Mater. Chem. Phys.* 139 (2013) 1-7.

[42] M. Esthaku Peter, P. Ramasamy, "Growth, thermal, dielectric and mechanical studies of triglycine zinc chloride, a semiorganic nonlinear optical material," *Mater Lett.* 64 (2010) 1–3.

[43] E. Meyer, Z.Ver, "Contribution to the Knowledge of Hardness and Hardness Testing," *Dtsch. Ing*, 52 (1908) 645–654.

[44] E.M. Onistch, "Micro-hardness Testing," *Mikroskopie* 95 (1950) 12-14

[45] P. Mythili, T. Kanagasekaran, R. Gopala Krishnan, "Investigations on nucleation kinetics, growth and characterization of sulphanilic acid single crystals," *Cryst. Res. Technol.* 42 (2007) 791–799.

[46] J.P. Chaoon, W.H. Broughton, A.R. Katzuk, "The determination of yield strength from hardness measurements," *Metall. Trans.* 2 (1971) 1979–1983.

[47] M.Sheik-Bahae, A.A.Said, E.W.Van Stryland, "High-sensitivity, single-beam n_2 measurements," *Opt. Lett.* 14 (1989) 955-957.

[48] M.Sheik-Bahae, A.A. Said, T.H.Wei, D.J.Hagan, E.W.Van Stryland, "Sensitive measurement of optical nonlinearities using a single beam," *IEEE J.Quantum Electron.* 26 (1990) 760-769.

[49] N.Sudharshana, B.Keerthana, R.Nagalakshmi, V.Krishnakumar, L.Guru Prasad, "Growth and characterization of hydroxyethylammonium picrate single crystals for third-order nonlinear optical applications," *Mater. Chem. Phys.* 134 (2012) 736-746.

[50] M.D. Zidan, A. Arfan, A. Allahham, "Nonlinear optical study of 1-(carboxymethyl)-8-hydroxyquinolin-1-ium chloride and 1-(carboxymethyl)quinolin-1-ium chloride salts by Z-scan technique," *Opt. Laser Technol.* 86 (2016) 79–84.

[51] J. Mohana, G. Ahila, M. Divya Bharathi, G. Anbalagan, "Growth, spectral, optical, thermal, and mechanical behaviour of an organic single crystal: Quinolinium 2-carboxy 6-nitrophthalate monohydrate," *J. Cryst. Growth* 450 (2016) 181–189.

[52] M. Divya Bharathi , G. Ahila , J. Mohana, G. Chakkaravarthi , G. Anbalagan, "Synthesis, crystal structure, growth, optical and third order nonlinear optical studies of 8HQ2C5N single crystal - An efficient third-order nonlinear optical material," *Mater. Chem. Phys.* 192 (2017) 215-227.

[53] A.Subhasini, R.Kumaravel, S.Leela, H.S.Evans, D.Sastikumar, K.Ramamurthi, "Synthesis, growth and characterization of 4-bromo-4 chloro benzylidene aniline-A third order nonlinear optical material," *Spectrochim. Acta A* 78 (2011) 935-941.

[54] Raghavendra Bairy, Parutagouda shankaragouda Patil, Shivaraj R. Maidur, H. Vijeth, M.S. Murari ,K. Udaya Bhat , "The role of cobalt doping in tuning the band gap, surface morphology and third-order optical nonlinearities of ZnO nanostructures for NLO device applications", *RSC Adv.* 9 (2019) 22302 - 22312.

[55] J. Tingjian, H. Tingchao, L. Pengwei, M. Yujun, C. Yuting, "A study of the thermal-induced nonlinearity of Au and Ag colloids prepared by the chemical reaction method", *Optics Laser Technol*. 40 (2008) 936–940.

[56] F. Nasseri, E. Rokhsat, D. Dorranian, "Low power continues wave nonlinear optics in red BS dye doped PVA thin film", *Optik* 127 (2016) 6813-6820.

[57] F. L. S. Cuppo, A. M. Figueiredo Neto, S. L. Go'mez and P. Palffy-Muhoray, "Thermal-lens model compared with the Sheik-Bahae formalism in interpreting Z-scan experiments on lyotropic liquid crystals", *J. Opt. Soc. Am. B,* 19 (2002) 1342 - 1348.

[58] Z. Li, F. Gao, Z. Xiao, G. Ao, X.I. Wu, Y. Fang, Zhongquan Nie, T. Wei, J. Yang, Y. Wang, X. Zhang, J. Zuo, Y. Song, "Synthesis and third-order nonlinear optical properties of a sandwichtype mixed (phthalocyaninato)(schiff-base) triple-decker complexes," *Dyes Pigment*. 119 (2015) 70-80.

[59] X. Wang, C. Liu, Q. Gong, Y. Huang, C. Huang, "Anomalous heavy atom effect on optical limiting property of homoleptic double-decked sandwich-type lanthanide diphthalocyanines," *Opt. Commun.* 197 (2001) 83-87.

[60] N. Sheng, Z.D. Yuan, J.X. Wang, W.D. Chen, J. Sun, Y.Z. Bian, "Third-order nonlinear optical properties of sandwich-type mixed (phthalocyaninato)(porphyrinato) europium double- and triple-decker complexes," *Dyes Pigment.* 95 (2012) 627-631.

[61] C. Huang, K. Wang, J. Sun, J. Jiang, "Planar binuclear phthalocyanine-containing sandwich type rare-earth complexes: synthesis, spectroscopy, electrochemistry and NLO properties", *Eur. J. Inorg. Chem.* 9 (2014) 1546.

[62] Zhong-Jun Zhou, Guang-Tao Yu, Fang Ma, Xu-Ri Huang, Zhi-Jian Wu , Zhi-Ru Li, "Theoretical investigation on nonlinear optical properties of carbon nanotubes with Stone–Wales defect rings," *J. Mater. Chem. C* 2 (2014) 306–311.

[63] F. Castet, B. Champagne, "Assessment of DFT exchange-correlation functionals for evaluating the multipolar contributions to the quadratic nonlinear optical responses of small reference molecules," *J. Chem. Theory Comput*. 8 (2012) 2044–2052.

[64] A. Migalska-Zalas, "Theoretical simulation of the third order nonlinear optical properties of some selected organometallics complexes," *Digest J Nanomater Biostructures* 3 (2008) 1-8.

[65] M.T. Zhao, B.P. Singh, P.N. Prasad, "A systematic study of polarizability and microscopic third-order optical nonlinearity inthiophene oligomers," *J. Chem. Phys.* 89 (1988) 5535–5541.

[66] M. A. D. Oliveira, H. A. Duarte, J. -M. Pernaut and W. B. D. Almeida, "Energy Gaps of α,α'-Substituted Oligothiophenes from Semiempirical, Ab-initio, and Density Functional Methods," *J. Phys. Chem. A* 104 (2000) 8256-8262.

[67] H. Alyar, "A review on nonlinear optical properties of donor - accpetor derivatives of naphthalene and azanaphthalene," *Rev. Adv. Mater. Sci.* 34 (2013) 79–87.

[68] Yang Bai, Zhong-Jun Zhou, Jia-Jun Wang, Ying Li, Di Wu, Wei Chen, Zhi-Ru Li, Chia-Chung Sun, "The effects of external electric field: creating non-zero first hyperpolarizability for centrosymmetric benzene and strongly enhancing first hyperpolarizability for non-centrosymmetric edge-modified graphene ribbon H2N-(3, 3)ZGNR-NO2," *J. Mol. Model.* 19 (2013) 3983 – 3991.

[69] Haipeng Li, Hu Xu, Xiaopeng Shen, Kui Han, Zetong Bi & Runfeng Xu, "Size-, electric-field-, and frequency dependent third-order nonlinear optical properties of hydrogenated silicon nanoclusters," *Scientific Reports*, 6 (2016) 28067

[70] C.J. Bennet, F.D.Gnanam, "Dielectric studies on sodium fluoroantimonate single crystals," *Cryst. Res. Technol*. 29 (1994) 707-712.

[71] K.B.R. Varma, K.V.Rao, "Linear electrooptic effect in doped KDP crystals," *Bull. Mater. Sci.* 5 (1983) 39-48.

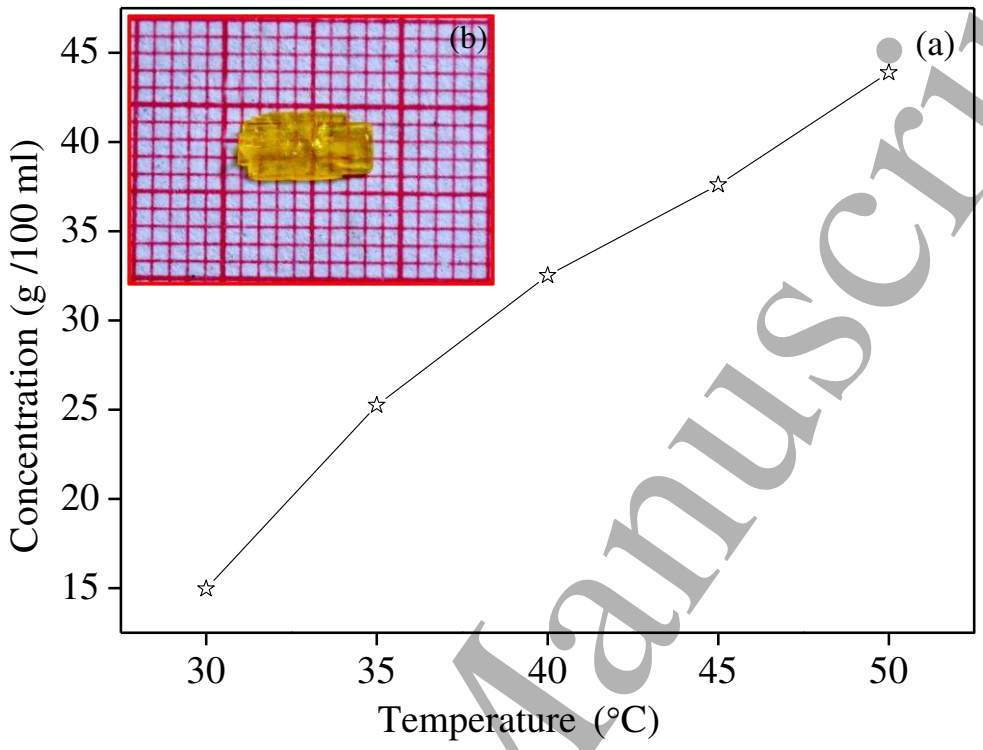

Fig.1(a). Solubility curve of 8-HQCN in ethanol and **(b).**As grown crystal of 8-HQCN (inset)

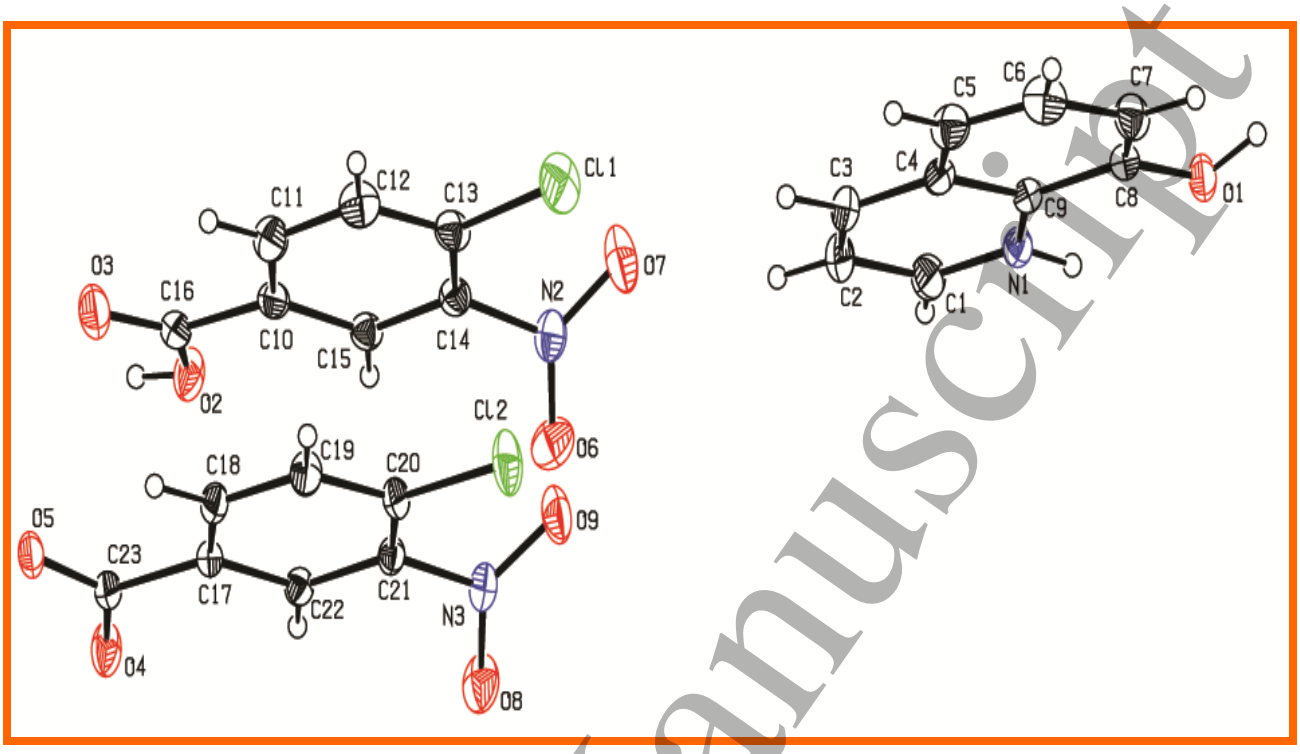

Fig.2. Molecular structure of 8-HQCN crystal

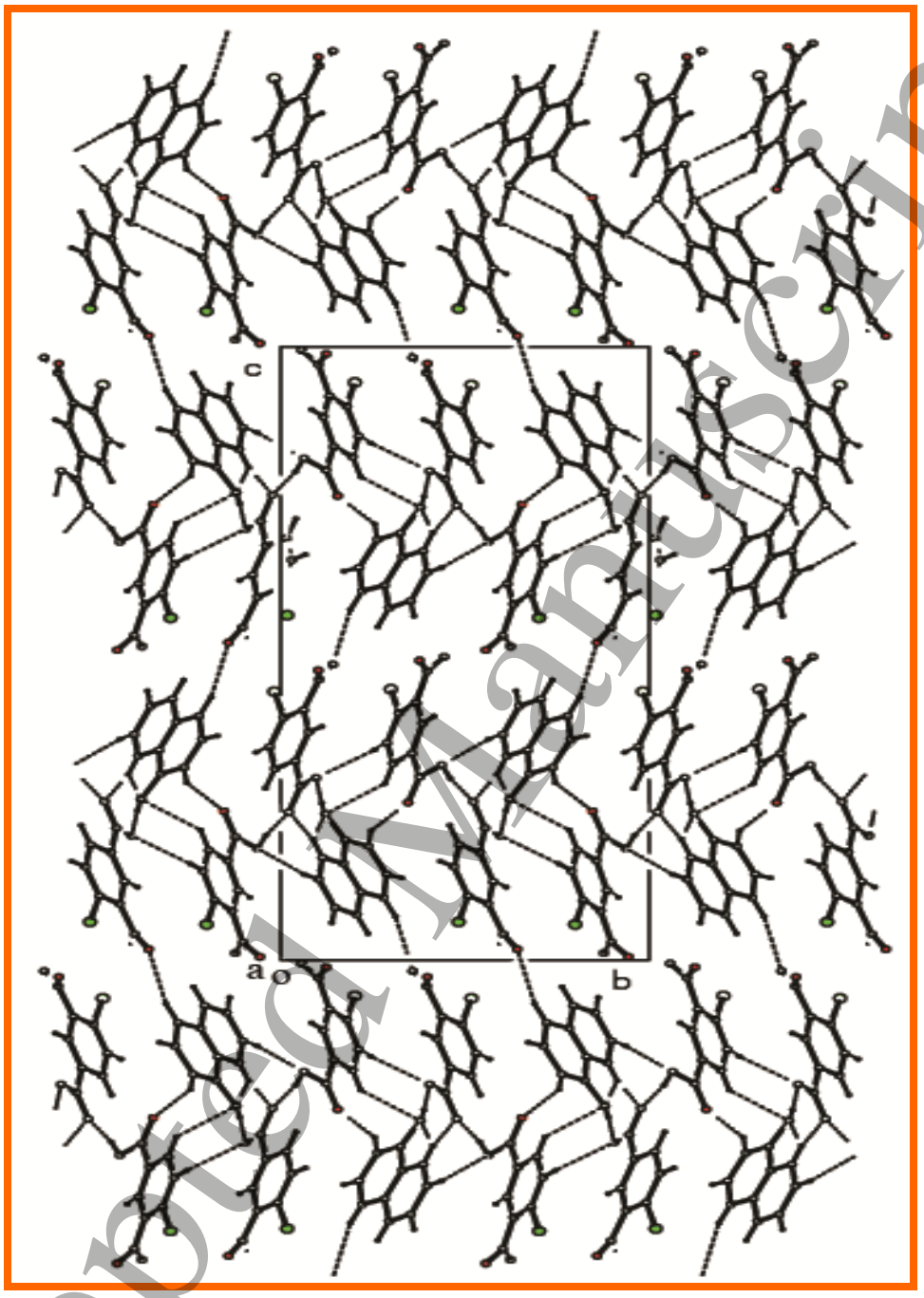

Fig. 3. Crystal structure packing viewed along the c axis

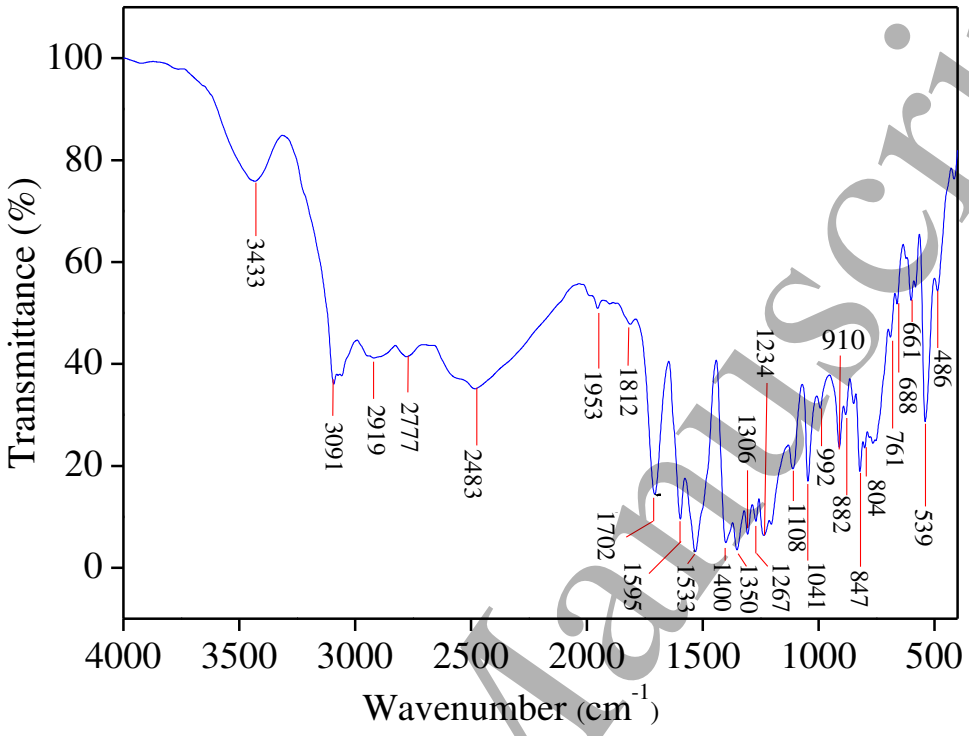

Fig. 4. FT-IR spectrum of 8-HQCN crystal

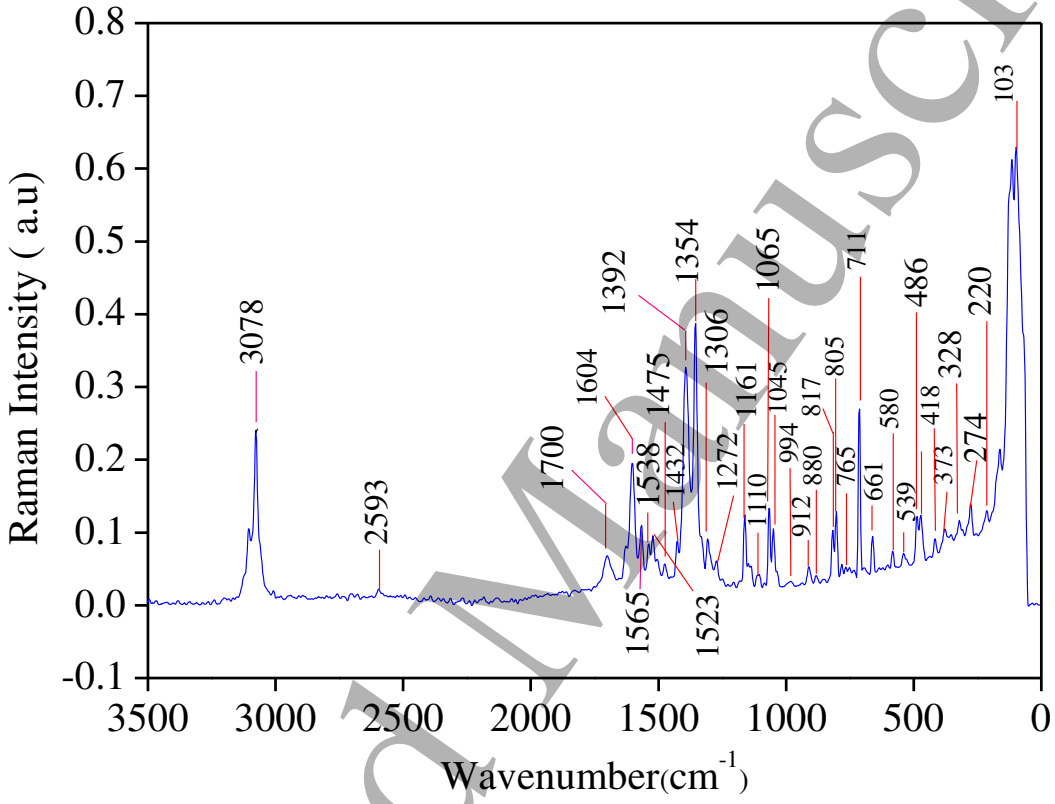

Fig. 5. FT-Raman spectrum of 8-HQCN crystal

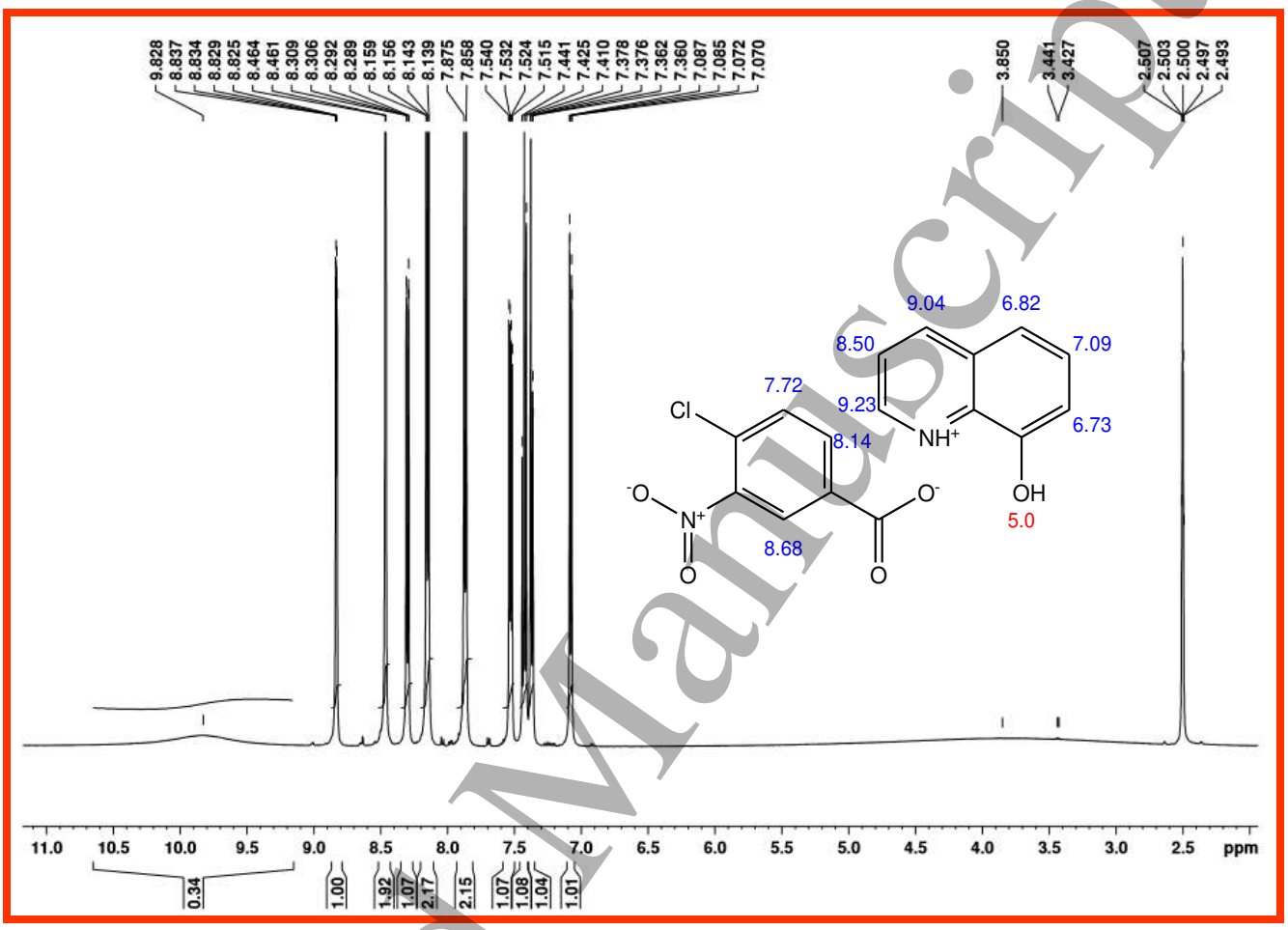

Fig. 6. ^{1}H NMR of 8-HQCN compound

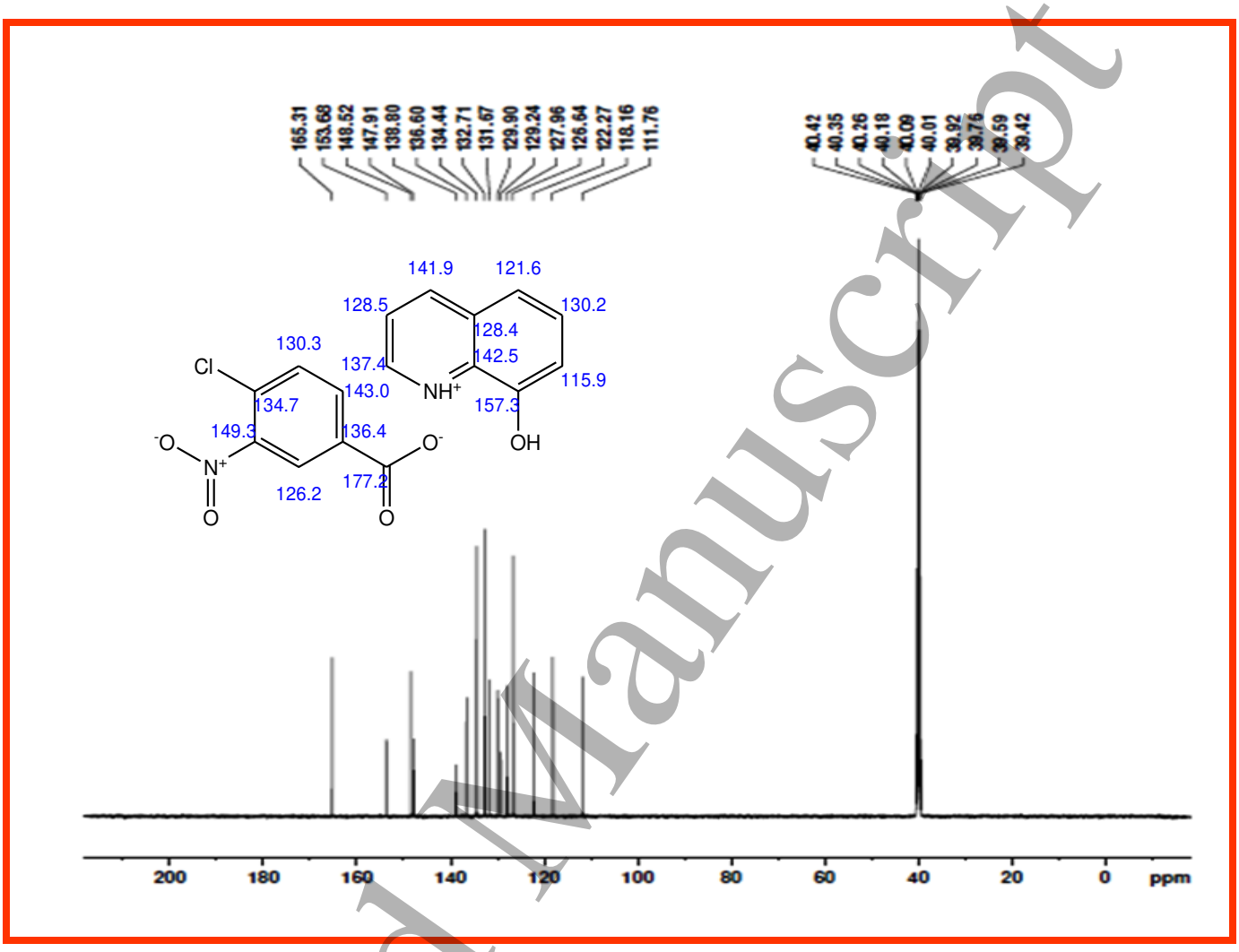

Fig. 7. ^{13}C NMR representation of 8-HQCN compound

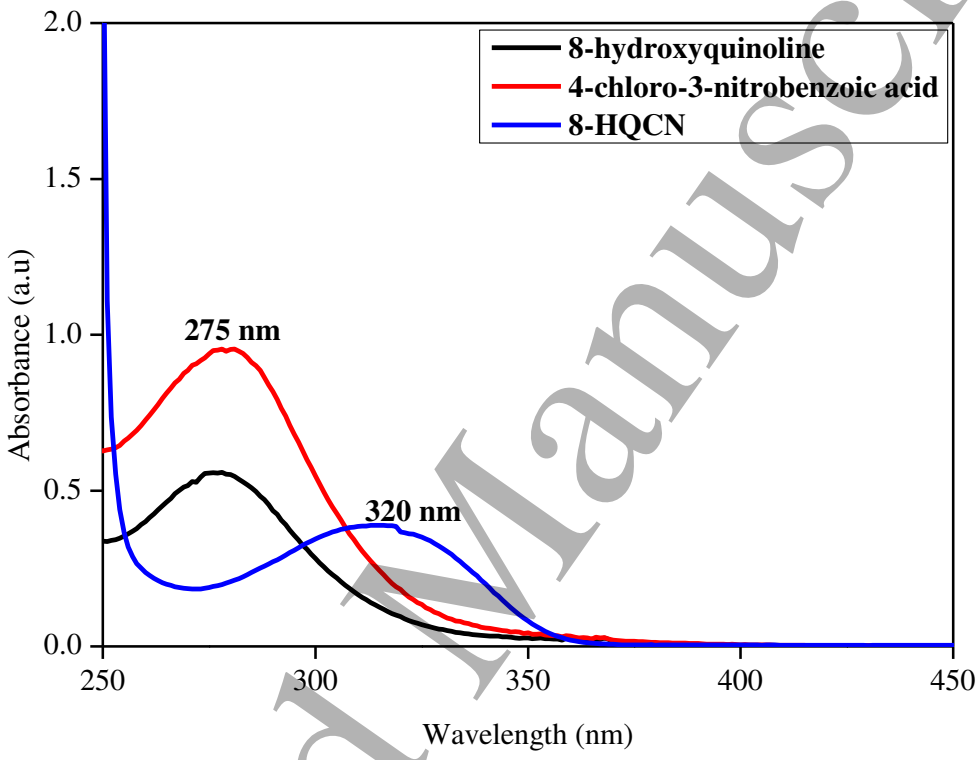

Fig. 8 (a). Absorbance spectrum of 8-HQ, 4C3N and 8-HQCN crystal

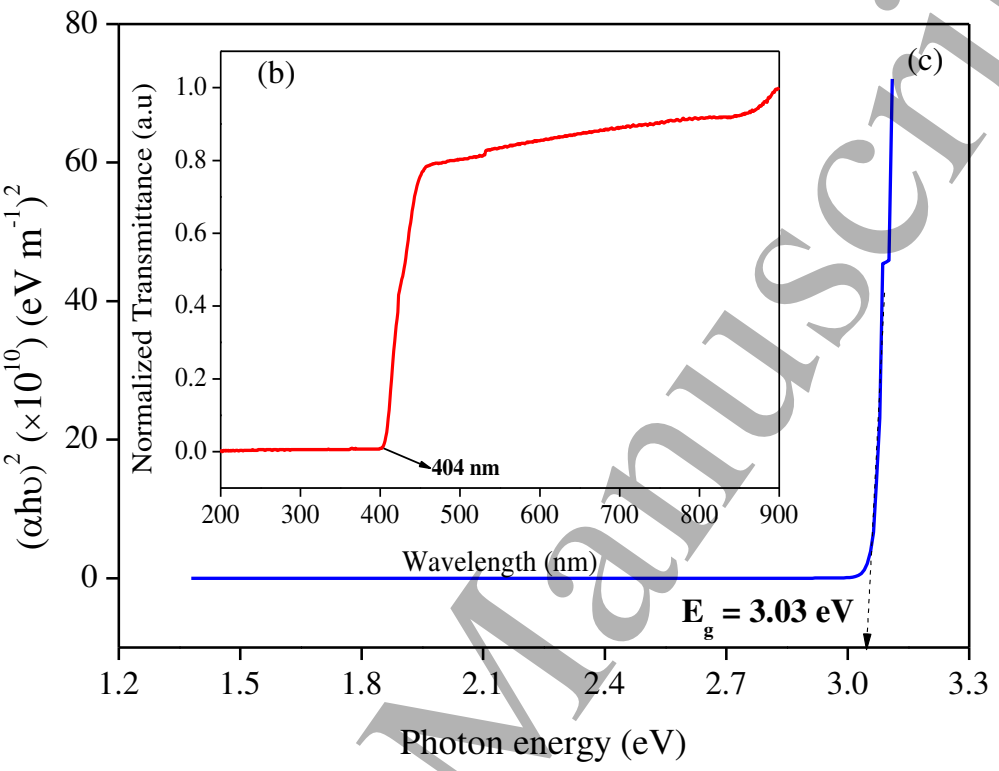

Fig. 8(b). The transmission spectrum and **(c)** Tauc's plot of 8-HQCN crystal along the (−100) plane

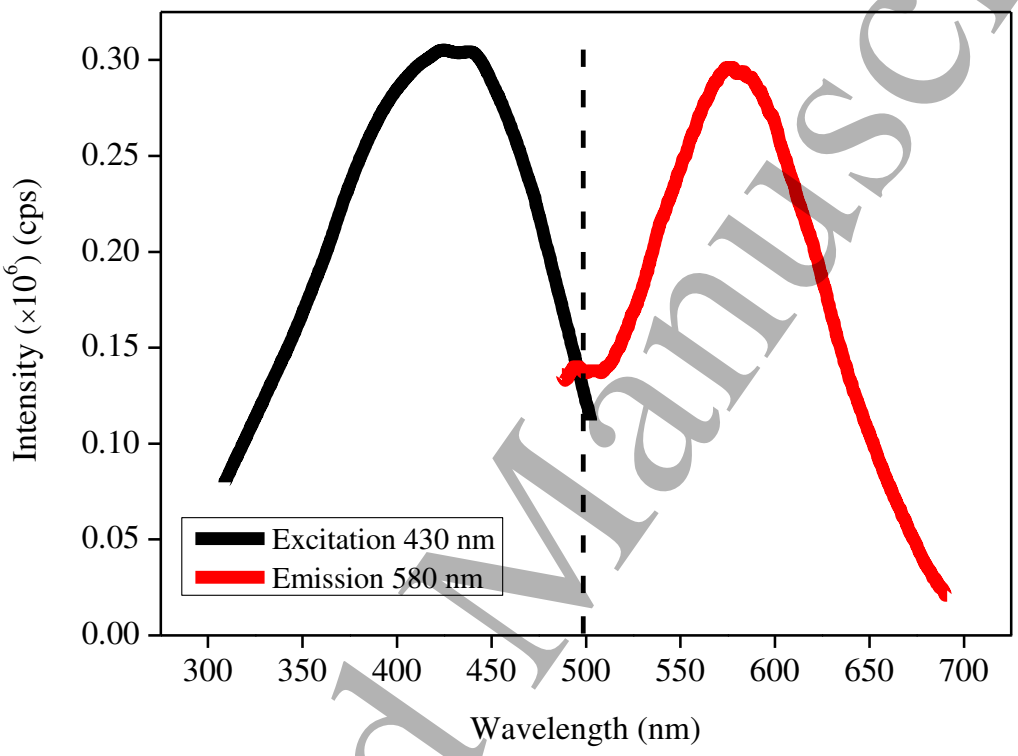

Fig. 9. Photoluminescence spectrum excited with 430 nm radiation for 8-HQCN

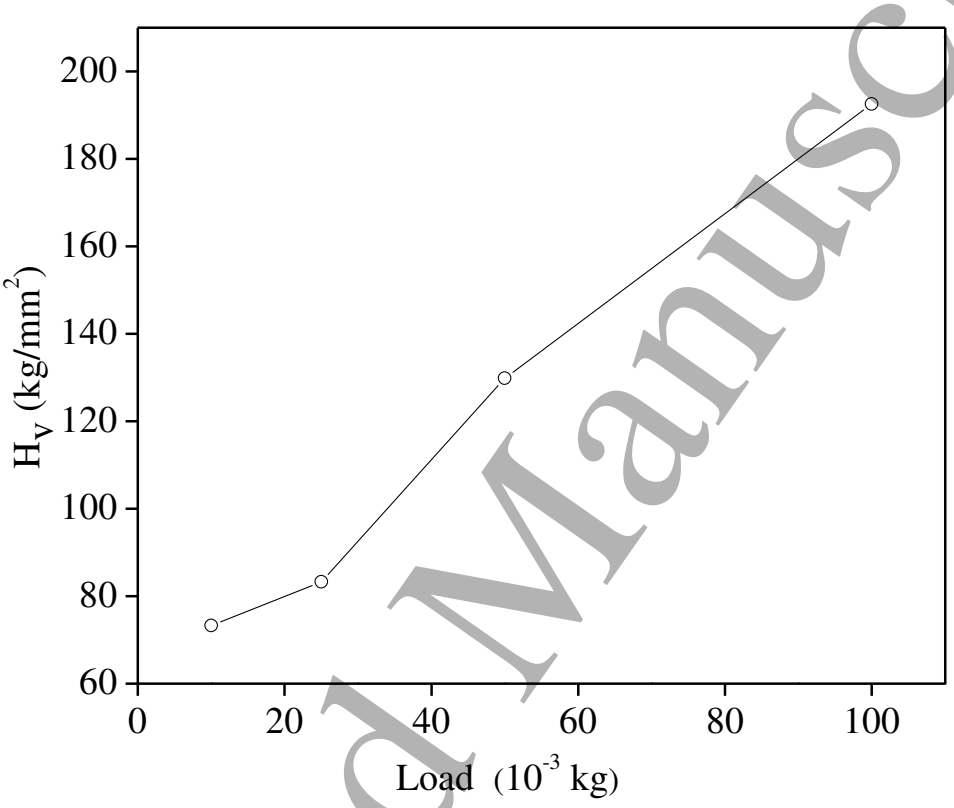

Fig.10 (a) Variation of Hv with load of 8-HQCN crystal

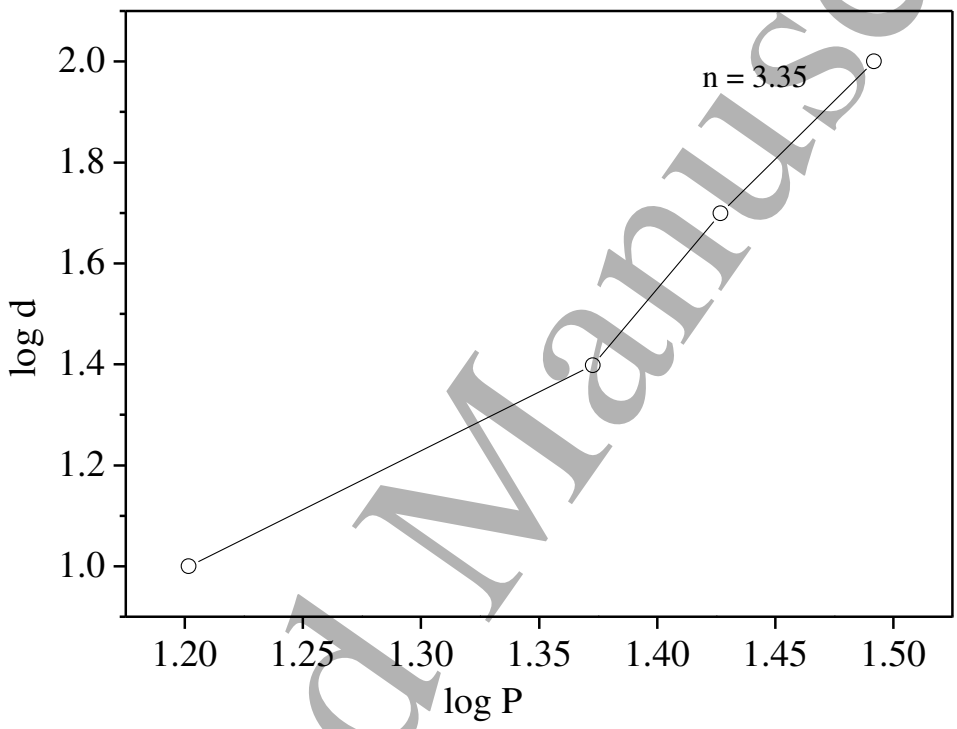

Fig.10 (b). Variation of log P vs. log d of 8-HQCN crystal

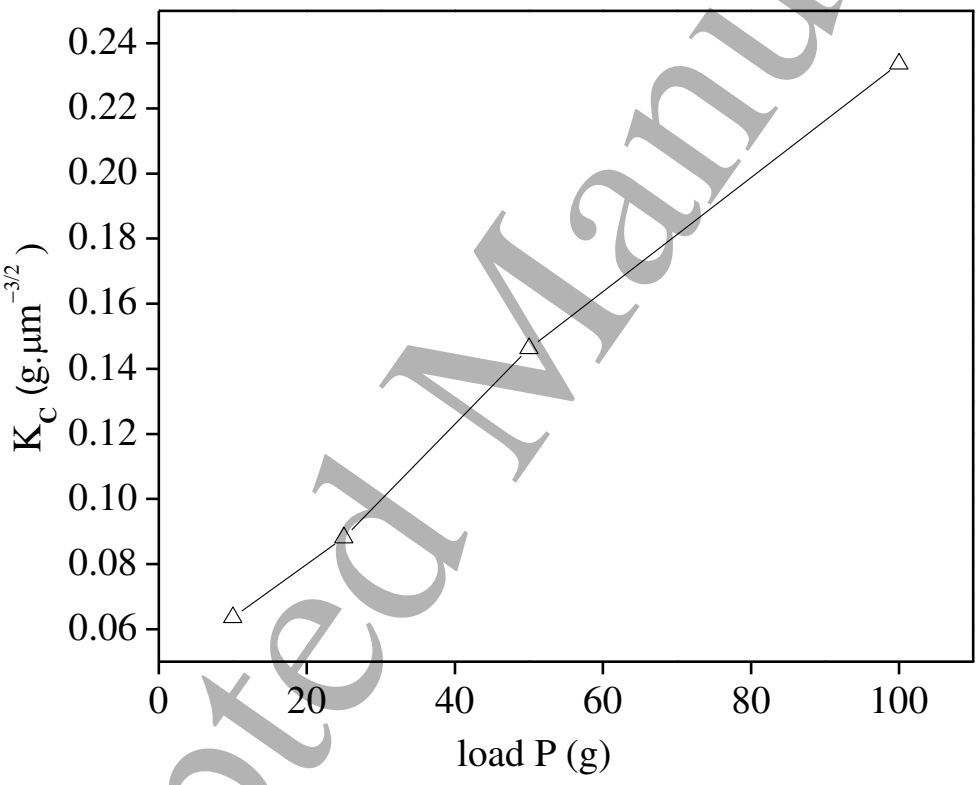

Fig.11 (a). The variation of Kc value at each load of 8-HQCN crystal

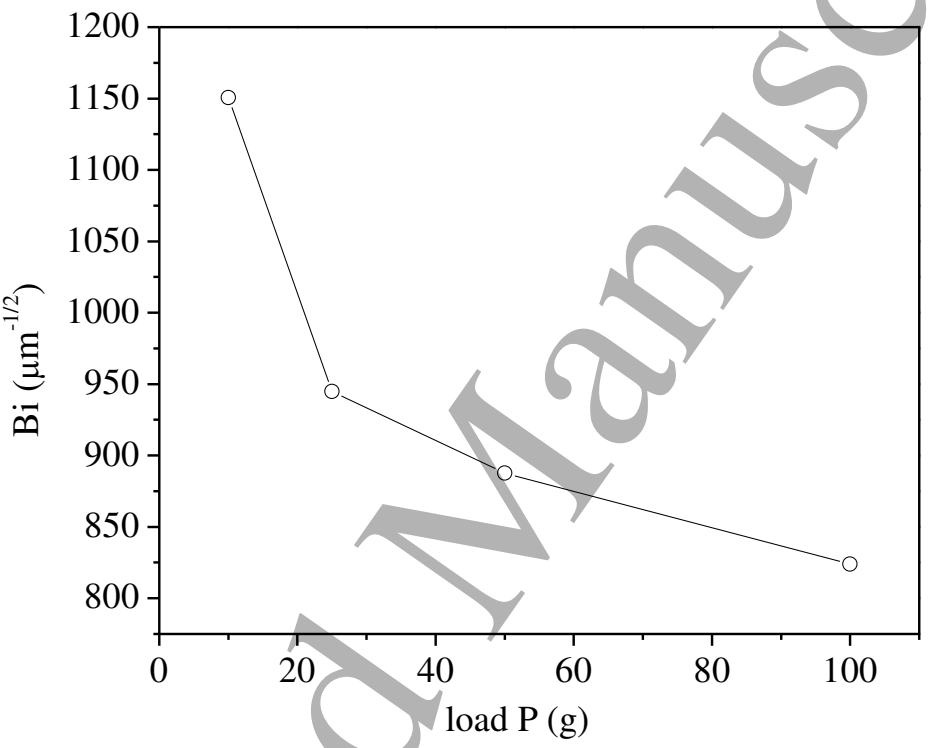

Fig.11 (b). The variation of brittleness index with load for 8-HQCN crystal

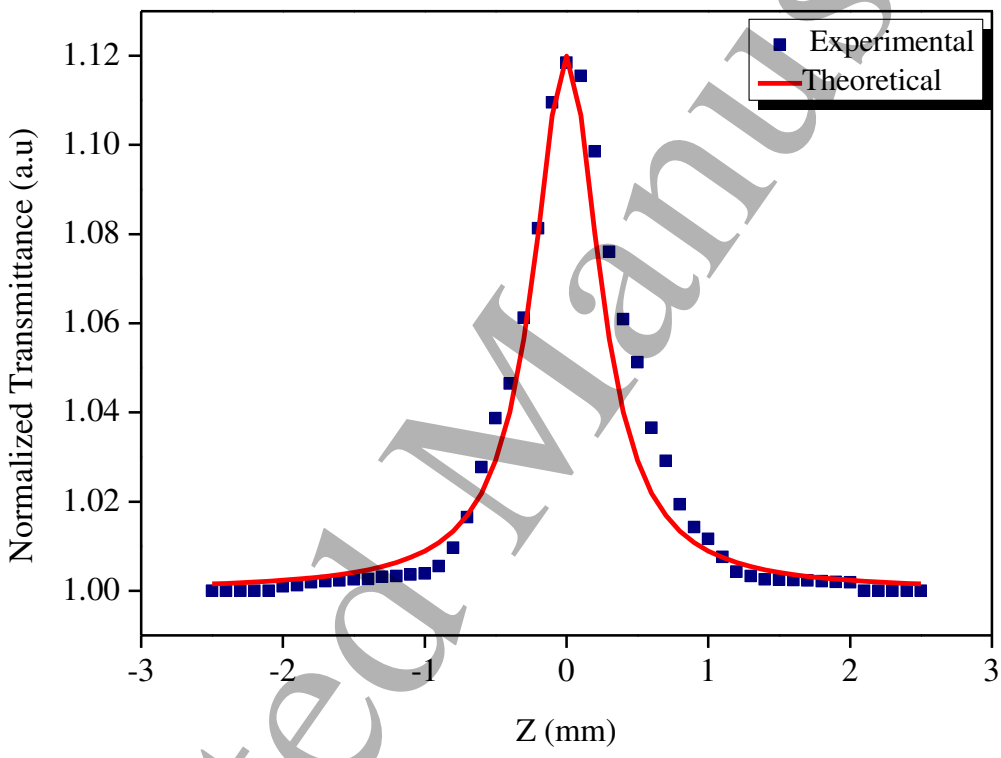

Fig. 12. Z-scan curve for open aperture of 8-HQCN crystal

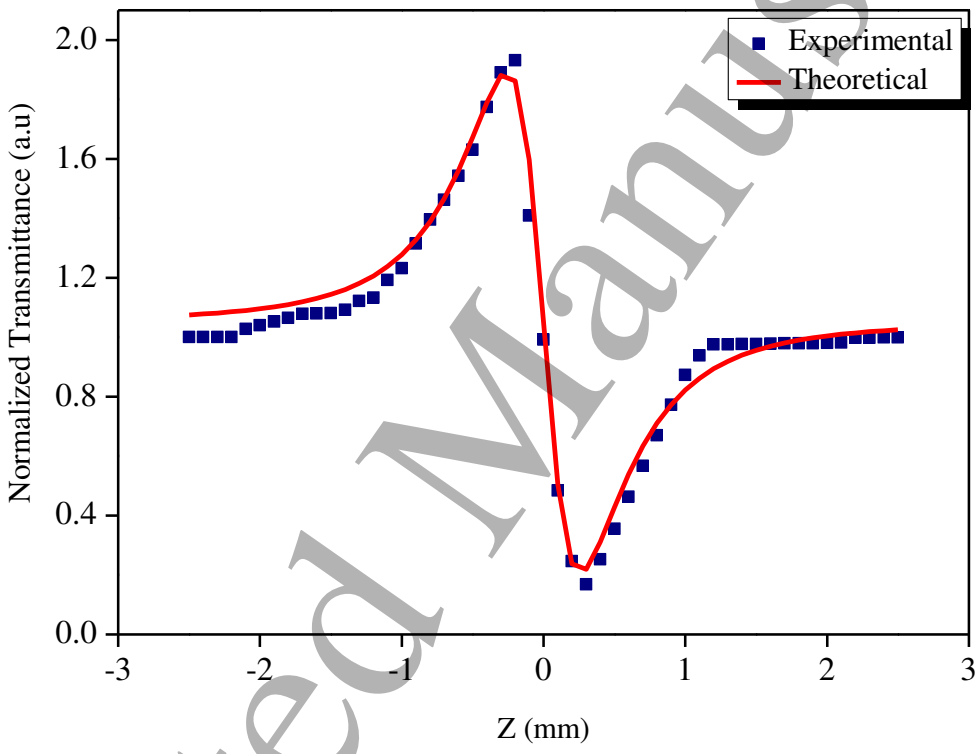

Fig. 13. Z-scan curve for closed aperture of 8-HQCN crystal

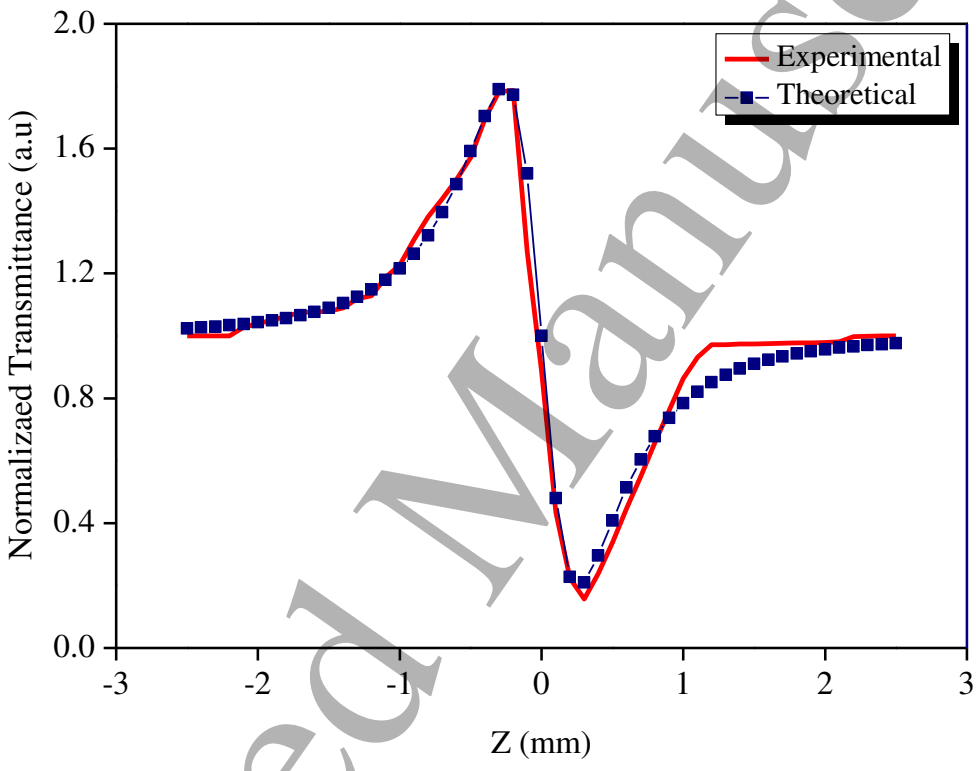

Fig. 14. Ratio of open and closed aperture Z-scan curve

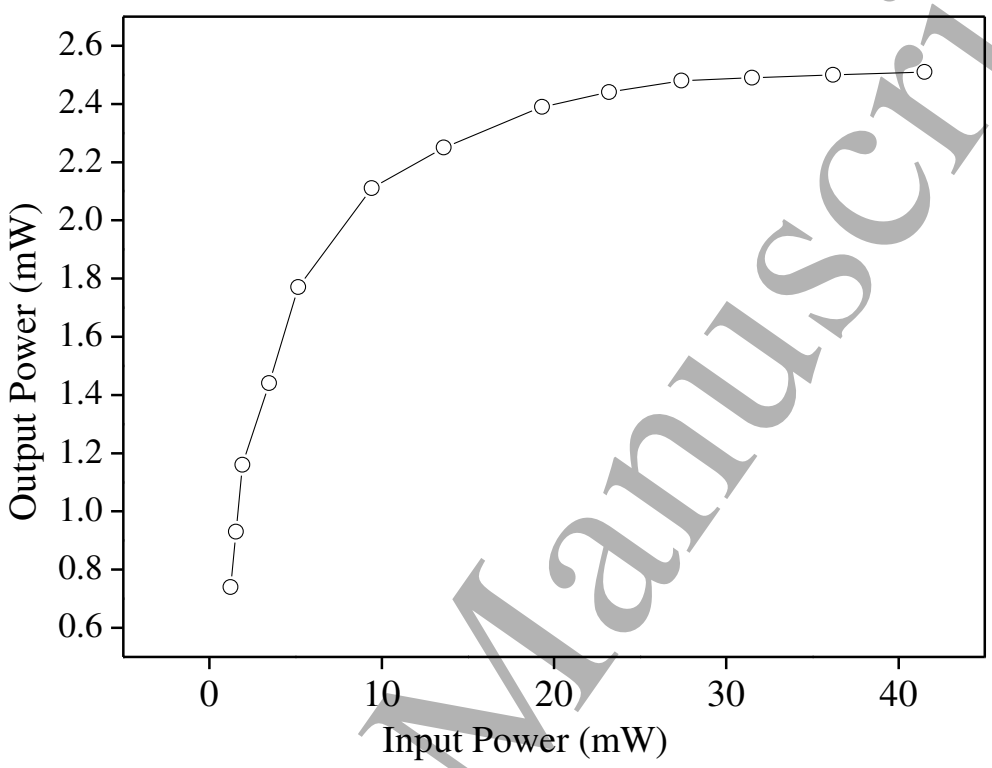

Fig. 15. Optical limiting curve for 8-HQCN

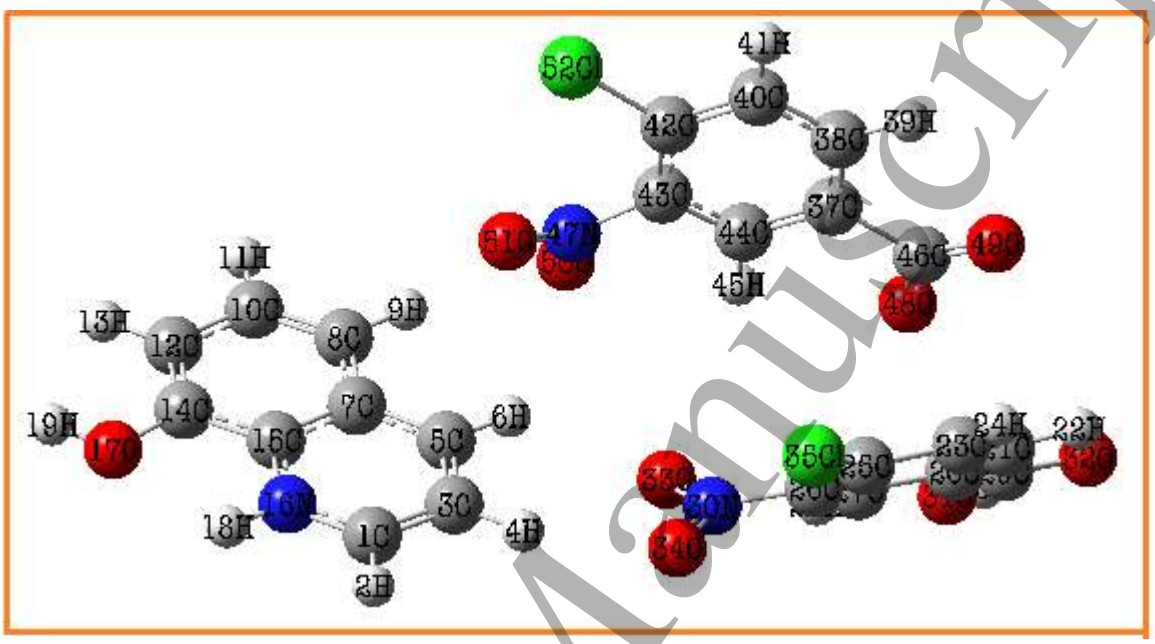

Fig.16. Optimized geometry of 8-HQCN with cam-b3lyp/6-311G(d,p) level

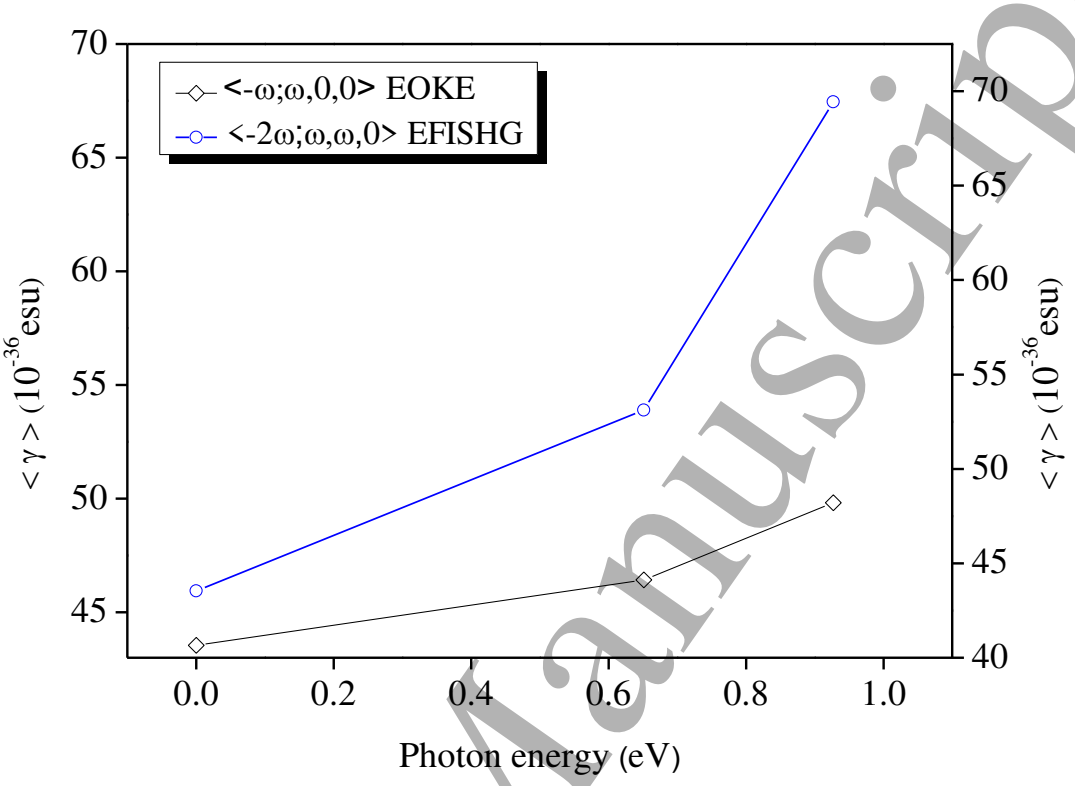

Fig.17. Frequency dependence on <γ> of 8-HQCN for EOKE and EFISHG, respectively.

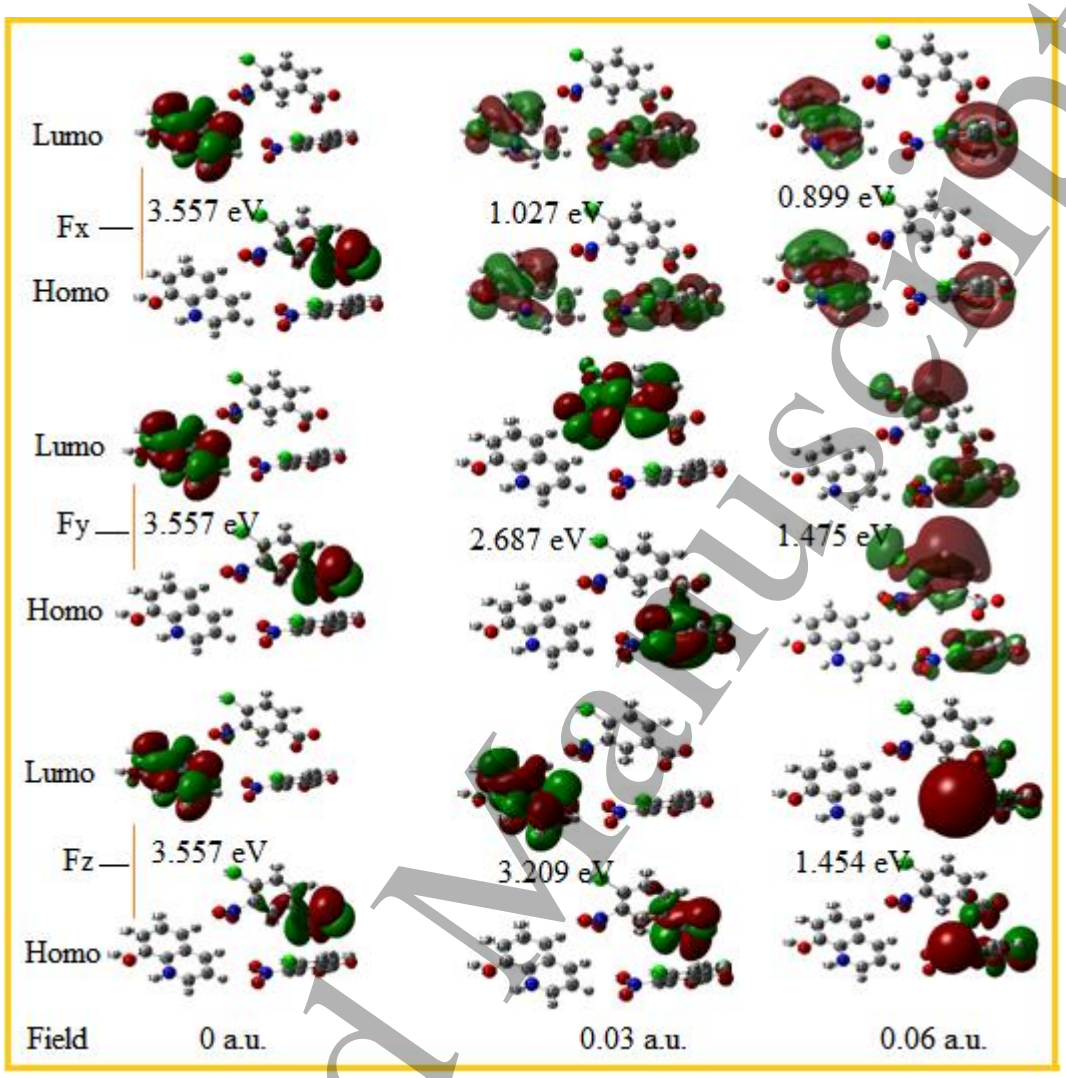

Fig.18. The molecular orbitals (MOs) of 8-HQCN under external electric fields along x,y and z directions. For electric fields, 1 au = 50 V/Å.

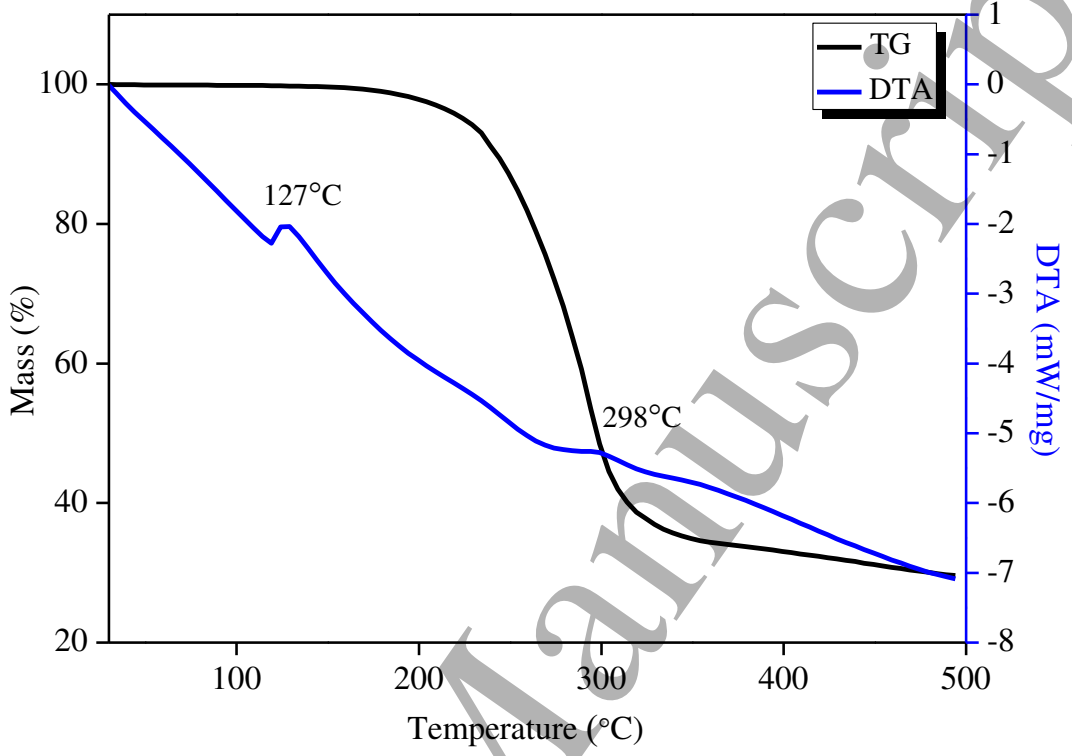

Fig. 19.TG-DTA thermogram of 8-HQCN crystal

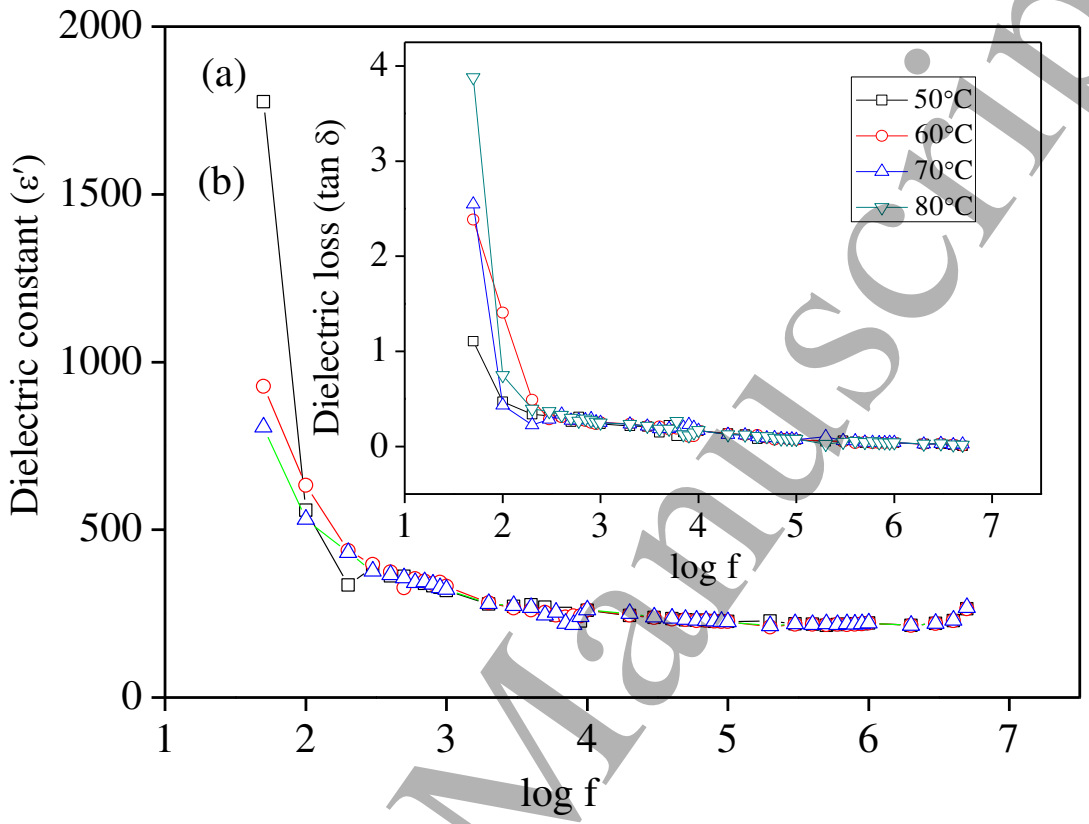

Fig.20 (a) Plot of showing the (a) dispersion of dielectric constant with frequency **(b)** the dielectric loss with frequency

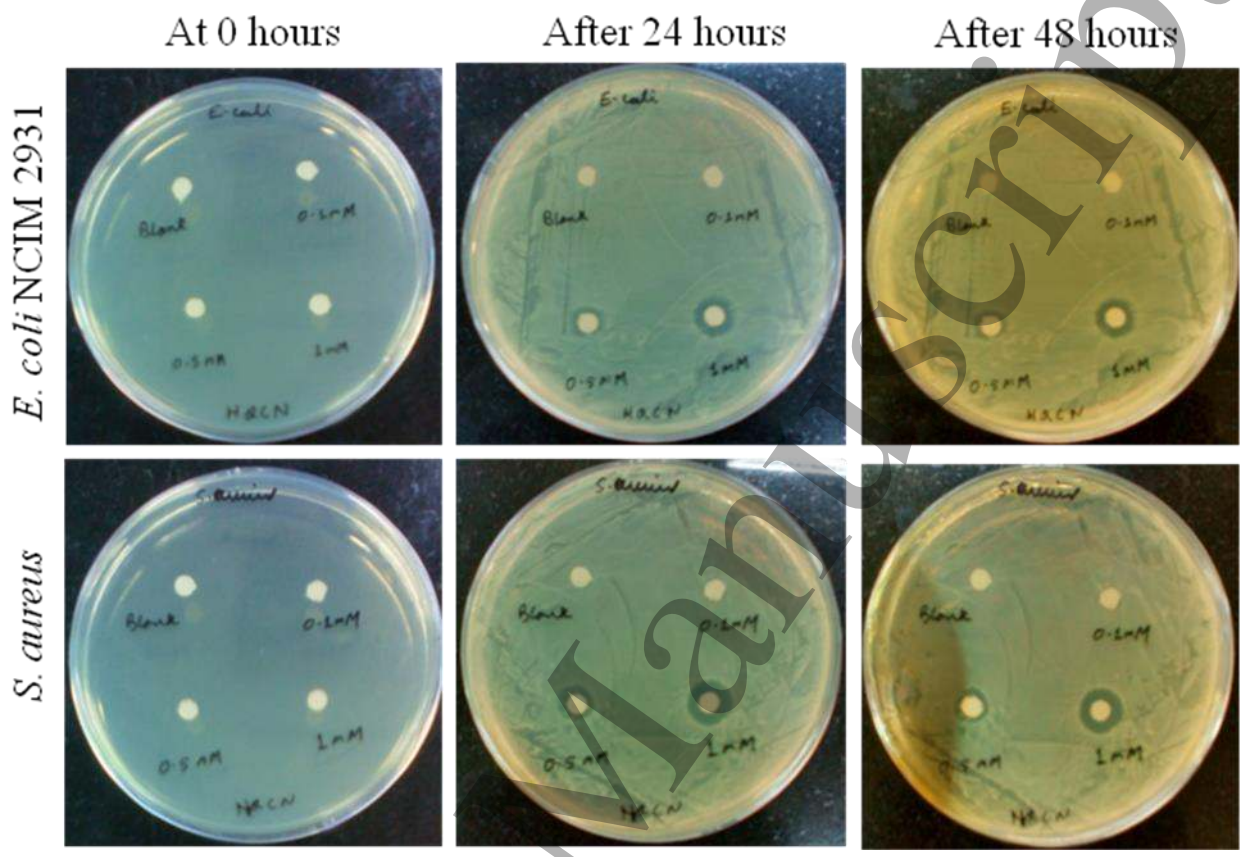

Fig. 21. Antibacterial activity of 8-HQCN

Table 1

Crystal data and structure refinement for 8-HQCN

Empirical formula	$C_{23}\ H_{15}\ Cl_2\ N_3\ O_9$	
Formula weight	548.28	
Temperature	295(2) K	
Wavelength	0.71073 Å	
Crystal system	Monoclinic	
Space group	$P2_1/n$	
Unit cell dimensions	a = 6.9806(2) Å	α= 90°
	b = 11.9919(4) Å	β= 92.5470(10)°
	c = 26.8872(8) Å	γ = 90°
Volume	2248.52(12) $Å^3$	
Z	4	
Density (calculated)	1.620 Mg/m^3	
Absorption coefficient	0.352 mm^{-1}	
F(000)	1120	
Crystal size	0.30 × 0.26 × 0.20 mm^3	
Theta range for data collection	1.52 to 27.16°	
Index ranges	-8<=h<=8, -14<=k<=15, -34<=l<=34	
Reflections collected	18779	
Independent reflections	4956 [R(int) = 0.0213]	
Completeness to theta = 27.16°	99.6 %	
Max. and min. transmission	0.9329 and 0.9016	
Refinement method	Full-matrix least-squares on F^2	
Data / restraints / parameters	4956 / 2 / 346	
Goodness-of-fit on F^2	1.079	
Final R indices [I>2sigma(I)]	R1 = 0.0379, wR2 = 0.0969	
R indices (all data)	R1 = 0.0475, wR2 = 0.1022	
Extinction coefficient	0.0033(5)	
Largest diff. peak and hole	0.309 and -0.346 $e.Å^{-3}$	

Table 2

Hydrogen bond geometry for 8-HQCN [Å and °]

D-H...A	D…H	H…A	D...A	D-H…A
N(1)-H(1)...O(1)	0.882(9)	2.37(2)	2.6908(18)	101.5(15)
C(2)-H(2)...O(7)	0.93	2.44	3.338(2)	161.3
N(1)-H(1)...O(5)i	0.882(9)	2.053(15)	2.8133(19)	143.8(18)
O(1)-H(1A)...O(4)ii	0.88(3)	1.73(3)	2.6137(17)	174(3)
C(7)-H(7)...O(3)ii	0.93	2.48	3.348(2)	154.6
O(2)-H(2A)...O(5)iii	0.830(10)	1.722(11)	2.5451(17)	171(3)
C(1)-H(1B)...O(2)iv	0.93	2.50	3.395(2)	161.4
C(5)-H(5)...O(9)v	0.93	2.58	3.489(2)	166.3
C(11)-H(11)...O(1)vi	0.93	2.53	3.291(2)	139.7

Symmetry codes: (i) x+1/2, -y+3/2, z-1/2 ; (ii) x+3/2, -y+3/2, z-1/2 ; (iii) x-1/2, y+1/2, -z+1/2 ; (iv) -x, -y+2, -z ; (v) x+1, y, z ; (vi) x-1/2, -y+3/2, z+1/2.

Table 3
Vibrational frequency assignments of 8-HQCN crystal.

FT-IR (cm^{-1})	FT-Raman (cm^{-1})	Assignments
3433	-	O-H stretching
3091	3078	N-H stretching
2919	-	C-H stretching
2777	-	C-H stretching
-	2593	C-H stretching
2483	-	C-H stretching
1953	-	C-H stretching
1812	-	C-H stretching
1702	1700	COOH stretching
1595	1604	COO^- asymmetric stretching
-	1565	C-H stretching
1533	1538	NO_2 asymmetric stretching
-	1523	C=C bending
-	1475	C=C stretching
1400	1432	COO^- symmetric stretching
1350	1392	NO_2 symmetric stretching
-	1354	C-H bending
1306	1306	Inplane O-H deformation
1267	1272	C-O stretching
1234	-	C-N stretching
-	1161	Ring C-H deformation
1108	1110	C-Cl stretching
-	1065	C-Cl stretching
1041	1045	C-Cl stretching
992	994	C-H in plane bending
910	912	C-N deformation

882	880	C-N stretching
847	-	C-H out of plane bending
-	817	Ring C-H stretching
804	805	C-N stretching
761	765	C-H bending
-	711	C-H bending
688	-	C-H stretching
661	661	C=O deformation
597	580	C-O deformation
539	539	Rocking N=O
486	486	O-H inplane bending
-	418	C-C-C out of plane bending
-	373	C-N inplane bending
-	328	C-N stretching
-	274	C-N deformation
-	220	C-C-C out of plane bending
-	115	Lattice vibrations
-	103	Lattice vibrations

Table 4. Mechanical properties of 8-HQCN crystal

Load (g)	Hv (kg/mm^2)	N	K_C (g/μm$^{3/2}$)	B_i (μm$^{-1/2}$)	σ_y (kg/mm^2)	$C_{11}\times10^4$ (GPa)
10	73.2455	3.35	0.0636	1150.538	24.4151	1.833
25	83.2838	3.35	0.0881	944.845	27.7612	2.296
50	129.8107	3.35	0.1462	887.750	43.270	4.992
100	192.5127	3.35	0.2336	823.797	64.170	9.949

Table 5

Nonlinear optical parameters obtained from z-scan measurements

Parameters	Values
Laser beam wavelength	532 nm
Lens focal length (f)	3.5 cm
Optical path length	85 cm
Radius of the laser spot before the aperture (w_a)	15.84 μm
Aperture radius (r_a)	1 mm
Sample thickness (L)	0.5 mm
Effective thickness (L_{eff})	2.040×10^{-3} m
Linear absorption coefficient (α)	5.49×10^{-2} m
Linear refractive index (n_o)	3.05
Nonlinear refractive index (n_2)	9.75×10^{-8} cm^2/W
Nonlinear absorption coefficient (β)	0.10×10^{-4} cm/W
Real part of the third-order susceptibility	16.77×10^{-6} esu
Imaginary part of third order susceptibility	0.62×10^{-6} esu
Third order nonlinear susceptibility (χ^3)	16.78×10^{-6} esu

Table 6

Comparison of nonlinear optical data with some related crystals

Compound	n_o	$n_2\times10^{-8}$ (cm^2/W)	$\beta\times10^{-4}$ (cm)	$Re\chi^{(3)}\times10^{-7}$ (esu)	$Im\chi^{(3)}\times10^{-5}$ (esu)	Reference
8-hydroxyquinolinium (Z)-3-carboxyacrylate (II)	1.3616	1.91	6.56	9.02	1.56	[14]
8-hydroxyquinolinium 2-chloroacetate(I)	1.3624	0.41	8.54	1.94	2.03	[14]
1-(carboxymethyl)-8-hydroxyquinolin-1-ium chloride	1.3621	-4.66	8.37	21.9	1.99	[52]
Quinolinium 2-carboxy-6-nitrophthalate monohydrate	1.7923	1.176	-4.59	2.08	-4.09	[53]
8-hydroxyquinolinium 2-chloro-5-nitrobenzoate dihydrate	2.8100	7.23	2.04	4.46	2.51	[54]
8-HQCN	3.05	9.75	0.10	16.77	0.62	Present work

Table 7. Field dependent Third order susceptibility of 8-HQCN along x,y and z axis

Second order hyperpolarizability ($\times 10^{36}$esu)	λ (nm)	Third order nonlinear susceptibility $\chi^{(3)}\times10^{-6}$esu					
		F_x= 0.03 a.u	F_x= 0.06 a.u	F_y=0.03 a.u	F_y=0.06 a.u	F_z = 0.03 a.u	F_z =0.06 a.u
γ (0;0,0,0)	0	21.09	77.98	96.5	-677442	9.16	59.86
γ (-ω;ω,0,0)	1907	127.9	17624.5	307.0	61599.3	10.76	8.78
γ (-2ω;ω,ω,0)	1907	-118.8	6202.8	430.2	19970.8	16.47	22.02

Table 8

Excited state energy, oscillator strength and major contribution for orbits obtained at td- hf/6-311g (d, p) level

n	Energy (eV)	Wavelength (nm)	Oscillator strength ($k\times10^{-3}$)	Symmetry	Major contributions
1	4.8093	257.80	127.5	Singlet-A	H-6->LUMO (82%) (Nitrobenzoic)
4	5.1562	240.45	40.9	Singlet-A	H-8->LUMO (61%) 8-hydroxyquinoline H-6->L+1 (31%)
5	5.2538	235.98	91.7	Singlet-A	HOMO->L+3 (70%) 8-hydroxyquinoline
6	5.5369	223.92	54.2	Singlet-A	H-5->L+2 (59%) quinoline
8	5.6341	220.06	34.5	Singlet-A	H-7->L+2 (35%) quinoline
9	5.8995	210.16	6.5	Singlet-A	H-21->L+2 (30%)
12	6.3066	196.59	0.3	Singlet-A	H-9->L+4 (45%), H-9->L+23 (30%) NO_2
13	6.3298	195.87	1028	Singlet-A	H-6->L+1 (54%) NO_2
14	6.7053	184.90	423.3	Singlet-A	HOMO->L+8 (42%) (C=O)
17	6.8022	182.27	8.5	Singlet-A	HOMO->LUMO (71%) (C=O)
19	6.9426	178.58	936.7	Singlet-A	H-5->L+4 (47%) (C=O)
23	7.2279	171.53	0.9	Singlet-A	H-1->LUMO (86%)
24	7.3020	169.79	24.5	Singlet-A	H-1->L+3 (51%)
28	7.4960	165.40	0.2	Singlet-A	H-2->LUMO (86%)
29	7.5406	164.42	0.3	Singlet-A	H-4->LUMO (77%)
31	7.7103	160.80	11.4	Singlet-A	H-5->LUMO (88%) (C=O)

32	7.7788	159.38	0.2	Singlet-A	H-3->LUMO (79%) (C=O)
33	7.8122	158.70	5.5	Singlet-A	H-3->L+3 (47%) (C=O)
34	7.8254	158.43	5.2	Singlet-A	H-1->L+8 (42%) (C=O)
36	8.0284	154.43	5.1	Singlet-A	H-6->L+6 (71%) (C=O)
38	8.1450	152.22	5.3	Singlet-A	H-7->LUMO (71%) (C=O)
41	8.2799	149.74	0.0	Singlet-A	HOMO->L+1 (96%)
43	8.3375	148.70	30.6	Singlet-A	H-1->L+2 (62%)
44	8.4194	147.26	3.9	Singlet-A	H-6->L+7 (47%)
45	8.4634	146.49	3.0	Singlet-A	HOMO->L+2 (93%)

Table 9

Diameter of zone of inhibition coursed HQCN against bacteria

Bacterial species	Concentration (mM)	Diameter of zone of inhibition (mm)			Average diameter of zone of inhibition (mm)
E. coli NCIM 2931	0.1	0	0	0	0
	0.5	8	8.5	7.5	8±0.5
	1	10.5	10	10.5	10.33±0.28
S. aureus	0.1	0	0	0	0
	0.5	7.5	8	8	7.83±28
	1	10	10	10	10±0